



Kaunas University of Technology
Faculty of Mechanical Engineering and Design

Quality Evaluation of Hot Stamped Periodical Structures vs Adhesive Layer Properties

Master's Final Degree Project

Shubham Singhal

Project author

Assoc. prof. Eglė Fataraitė-Urbonienė

Supervisor

Kaunas, 2020



Kaunas University of Technology

Faculty of Mechanical Engineering and Design

Quality Evaluation of Hot Stamped Periodical Structures vs Adhesive Layer Properties

Master's Final Degree Project

Industrial Engineering and Management (6211EX018)

Shubham Singhal

Project author

**Assoc. prof. Eglė Fataraitė-
Urbonienė**

Supervisor

Prof. Sigitas Stanys

Reviewer

Kaunas, 2020



Kaunas University of Technology

Faculty of Mechanical Engineering and Design

Task of the Master's final degree project

Given to the student – Shubham Singhal

1. Title of the project –

Quality evaluation of hot stamped periodic structures vs adhesive layer properties

(In English)

Klijų sluoksnio savybių įtaka karštai perneštų periodinių struktūrų kokybei

(In Lithuanian)

2. Aim and tasks of the project –

Aim: To evaluate the quality of hot stamped periodic structures in dependence of adhesive layer nature and thickness.

Tasks:

1. To evaluate the influence of adhesive layer formation regimes on adhesive layer thickness;
2. To evaluate scratch resistance of adhesive layer vs adhesive layer formation regimes;
3. To evaluate quality of hot stamped structures in dependence of adhesive layer nature and hot stamping regimes.

3. Initial data of the project –

Not applicable

4. Main requirements and conditions –

Adhesive layer coating machine, profilometer, hot stamping device

Testing equipment: scratch tester, optical microscope, ImageJ analysis program.

Testing material: aluminium coated multilayer film with thickness, $h = 19\mu\text{m}$ and ordinary paper with grammage of 80g/m^2 .

Adhesives: Nolax S35.3197, Lotto OPU746, Nolax S35.3213 and solvent based.

Project author

Shubham Singhal

(Name, Surname)

(Signature)

(Date)

Supervisor

Assoc. prof. Eglė Fataraitė-
Urbonienė

(Name, Surname)

(Signature)

(Date)

Head of study
field programs

Assoc. prof. Regita Bendikiene

(Name, Surname)

(Signature)

(Date)

Shubham Singhal. Quality Evaluation of Hot Stamped Periodical Structures vs Adhesive Layer Properties. Master's Final Degree Project, supervisor Assoc. prof. Eglė Fataraitė-Urbonienė; Kaunas University of Technology, Faculty of Mechanical Engineering and Design.

Study field and area (study field group): Production Engineering (E10), Engineering Sciences (E).

Keywords: water based adhesives, solvent based adhesives, adhesion process, hot stamping, multilayered periodical structures, scratch test, thin film formation, quality evaluation.

Kaunas, 2020. 57 p.

Summary

With advancement of manufacturing technology and struggle to maintain the best adhesive quality, developers continuously make efforts to improve their production efficiency without hindering the quality of the adhesive. So, this research aims to incorporate the effect on quality of hot stamped periodical structures using different layer thicknesses and hot stamping regimes.

Four adhesives which differ in concentration and viscosity were used during this research. Three of them are water based (S35.3197 and S35.3213 (Nolax, Switzerland), OPU746 (Lotto, Germany)) and one is the solvent based TC-03 (Centro Grafico DG S.p.A, Italy). All four adhesives were applied on multilayered polymer film with embossed periodical structures using rods with different wire diameter ($d = 4, 14, 24, 50$ and $80 \mu\text{m}$) under similar conditions. It was observed that adhesives Nolax S35.3197 and Lotto OPU746 followed linear dependence on coating thickness while the other two showed variable patterns due to low viscosity.

To evaluate adhesive layer properties scratch test was conducted at five different loads, $S = 260.86\text{mN}, 290.28\text{mN}, 309.89\text{mN}, 329.5\text{mN}$ and 358.92mN with all other parameters being same, on adhesive layers and it was found that adhesive Nolax S35.3197 had minimum variation of data in comparison to others and in general, the scratch width increased with the increasing load.

Further, hot stamping was conducted on all samples for time, $t = 1\text{sec}$ at constant load on substrate with grammage of 80g/m^2 . It was found that hot stamping quality depends on adhesive layer nature, its thickness and hot stamping temperature. Based on visual inspection, best quality of stamped structures were found in case of adhesive layer A1 ($d=14\mu\text{m}, T=106^\circ\text{C}; d=24\mu\text{m} T=73^\circ, 90^\circ, 106^\circ\text{C}; d=50\mu\text{m}; T=73^\circ, 90^\circ\text{C}$) adhesive layer A2 ($d=14\mu\text{m}, T=106^\circ\text{C}; d=24\mu\text{m} T=106^\circ\text{C}; d=50\mu\text{m}; T=90^\circ, 106^\circ\text{C}$) and for adhesive A4 at rod diameter $d=50\mu\text{m}$ and hot stamping temperature $T=106^\circ\text{C}$. These structures were selected for final evaluation.

For scratch testing of hot stamped periodical structures, same loads were used with similar conditions as those for adhesive layer properties evaluation. It was found that at smaller loads, $S = 260.86$ and 290.28 mN , there is very small or no deformation observed while in case of higher loads, $S = 309.89, 329.5$ and 358.92 mN , adhesive or cohesive failure was observed.

Shubham Singhal. Klijų sluoksnio savybių įtaka karštai perneštų periodinių struktūrų kokybei. Magistro baigiamasis projektas, vadovė Assoc. prof. Eglė Fataraitė-Urbonienė; Kauno technologijos universitetas, Mechanikos inžinerijos ir dizaino fakultetas.

Studijų kryptis ir sritis (studijų krypčių grupė): Gamybos inžinerija (E10), Inžinerijos mokslai (E).

Reikšminiai žodžiai: vandens dispersiniai klėjai, tirpikliniai klėjai, karštas įspaudavimas, daugiasluoksnės polimerinės plėvelės, periodinės struktūros, brėžimo bandymas, plėvelės formavimas, kokybės vertinimas.

Kaunas, 2020. 57 p.

Santrauka

Šio darbo tikslas - įvertinti klijų sluoksnio kilmės, jo storio ir karšto įspaudavimo temperatūros įtaką daugiasluoksnėje polimerinėje plėvelėje suformuotų periodinių struktūrų kokybei.

Šiam tyrimui buvo naudojami skirtingos klampos ir koncentracijos vandens dispersiniai (S35.3197 and S35.3213 (Nolax, Šveicarija), OPU746 (Lotto, Vokietija)) ir 10 proc. koncentracijos tirpikliniai klėjai TC-03 (Centro Grafico DG S.p.A, Italija). Klijų sluoksnis ant daugiasluoksnės polimerinės plėvelės su išpaustomis periodinėmis struktūromis, buvo dengiamas naudojant strypus, kurių vielos skersmuo buvo $d = 4, 14, 24, 50$ ir $80 \mu\text{m}$). Pastebėta, kad klijų Nolax S35.3197 ir Lotto OPU746 atveju egzistuoja tiesinė priklausomybė tarp strypo vielos skersmens ir klijų sluoksnio storio. Tuo tarpu kitais atvejais aiškios priklausomybės nenustatyta.

Klijų sluoksnio savybėms įvertinti tiktas brėžimo bandymas pastovios apkrovos sąlygomis ($S = 260,86\text{mN}, 290,28\text{mN}, 309,89\text{mN}, 329,5\text{mN}$ ir $358,92\text{mN}$). Mažiausias brėžimo griovelio pločio kitimas gautas Nolax S35.3197 klijų atveju ir brėžimo griovelio plotis didėjo didėjant brėžimo apkrovai.

Karšto įspaudavimo procedūra atlikta esant $t = 1$ s presavimo trukmei ant popieriaus, kurio gramatūra yra $80 \text{ g} / \text{m}^2$. Nustatyta, kad karšto įspaudavimo kokybė priklauso nuo klijų sluoksnio kilmės, jo storio ir įspaudavimo temperatūros. Atlikus vizualinį vertinimą, geriausia įspaudavimo kokybė gauta esant šiems klėjams ir jų sluoksnio formavimo režimams: A1 ($d = 14\mu\text{m}, T = 106^\circ\text{C}; d = 24\mu\text{m} T = 73^\circ, 90^\circ, 106^\circ\text{C}; d = 50\mu\text{m}; T = 73^\circ, 90^\circ\text{C}$). A2 ($d = 14 \mu\text{m}, T = 106^\circ\text{C}; d = 24 \mu\text{m} T = 106^\circ\text{C}; d = 50 \mu\text{m}; T = 90^\circ, 106^\circ\text{C}$) ir A4, kai strypo skersmuo $d = 50 \mu\text{m}$, o karšto štampos temperatūra $T = 106^\circ\text{C}$. Šios struktūros buvo atrinkta galutiniam vertinimui.

Tikrinant karštai išpaustų periodinių struktūrų atsparumą brėžimui, buvo naudojamos tos pačios apkrovos, kaip ir klijų sluoksnio kokybės vertinimo atveju. Nustatyta, kad esant mažesnėms apkrovoms ($S = 260,86$ ir $290,28 \text{ mN}$) suformuotos struktūros deformacija yra labai maža arba jos nėra, o esant didesnėms apkrovoms - $S = 309,89, 329,5$ ir $358,92 \text{ mN}$, pastebėtas mišrus struktūros suardymas.

Table of Contents

List of Figures	7
List of Tables	8
Introduction	9
1. Review of Literature	10
1.1. Background.....	10
1.2. Theories of Adhesion	10
1.3. Multilayered structures.....	12
1.4. Water-based adhesives and adhesive testing	13
1.5. Adhesion test methods.....	15
1.5.1. Cross-cut method	15
1.5.2. Indentation debonding	16
1.5.3. Scratch test.....	16
2. Experimental part	18
2.1. Materials	18
2.1.1. Polymeric substrate	18
2.1.2. Adhesives.....	18
2.2. Adhesive layer formation	18
2.3. Adhesive layer thickness measuring	19
2.4. Optical microscopy	20
2.5. Scratch Testing.....	21
2.6. Groove Width determination	21
2.7. Hot stamping procedure	21
2.8. Hot stamping quality evaluation	22
2.9. Adhesion Evaluation	22
3. Results and discussions	23
3.1. Influence of adhesive nature on adhesive layer thickness	23
3.2. Evaluation of adhesive layer structure	24
3.3. Evaluation of adhesive properties between multilayer films and adhesives	28
3.4. Evaluation of quality of hot stamped periodical structures	38
4. Recommendations	53
5. Conclusion	54
6. List of References	56

List of Figures

Fig. 1. Classification of cross-cut (22).....	16
Fig. 2. Indentation debonding (23)	16
Fig. 3. Scratch test set-up (23).....	17
Fig. 4. Polymeric Foil Structure	18
Fig. 5. K printing proofer	19
Fig. 6. Coating thickness tester	20
Fig. 7. Optical Microscope.....	20
Fig. 8. Scratch test setup	21
Fig. 9. Hot stamping machine (1 - Temperature regulator; 2 - Press Lever; 3 - Stamping Die; 4 - Stamping Bed).....	22
Fig. 10. Graph between rod diameter vs adhesive layer thickness.....	23
Fig. 11. Multilayer structures for sample adhesive A1 at rod diameter 4 μ m under scratch loads (a) – 309.89mN (b) – 290.28mN (c) – 329.5mN (d) – 358.92mN (e) – Groove width (f) – Delaminated width	29
Fig. 12. Multilayer structures for sample adhesive A1 at rod diameter 14 μ m under scratch loads (a) – 309.89mN (b) – 290.28mN (c) – 260.86mN (d) – 329.5mN (e) – 358.92mN.....	30
Fig. 13. Multilayer structures for sample adhesive A1 at rod diameter 50 μ m under scratch loads (a) – 309.89mN (b) – 290.28mN (c) – 260.86mN (d) – 329.5mN (e) – 358.92mN.....	30
Fig. 14. Multilayer structures for sample adhesive A2 at rod diameter 4 μ m under scratch loads (a) – 309.89mN (b) – 290.28mN (c) – 260.86mN (d) – 329.5mN (e) – 358.92mN.....	31
Fig. 15. Multilayer structures for sample adhesive A2 at rod diameter 14 μ m under scratch loads (a) – 309.89mN (b) – 290.28mN (c) – 260.86mN (d) – 329.5mN (e) – 358.92mN (f) – Cohesion failure width.....	32
Fig. 16. Elastic deformation dimensions for scratch load (a) – 309.89mN (b) – 290.28mN (c) – 260.86mN (d) – 329.5mN (e) – 358.92mN.....	35
Fig. 17. Effect of scratch load on groove widths for multilayered structure with adhesive A1	36
Fig. 18. Effect of scratch load on groove widths for multilayered structure with adhesive A2	36
Fig. 19. Effect of scratch load on groove widths for multilayered structure with adhesive A3	37
Fig. 20. Effect of scratch load on groove widths for multilayered structure with adhesive A4	37

List of Tables

Table 1. Adhesives details	18
Table 2. Samples made by combination of adhesives and coating thickness.....	19
Table 3. Adhesive A1 surface analysis.....	24
Table 4. Adhesive A2 surface analysis.....	25
Table 5. Adhesive A3 surface analysis.....	26
Table 6. Adhesive A4 surface analysis.....	27
Table 7. Scratch profiles of samples with respect to scratch loads.....	32
Table 8. Typical views of hot stamped structures at temperatures 90°C, 106°C and 113°C	38
Table 9. Typical views of hot stamped structures at temperatures 73°C, 90°C and 106°C	39
Table 10. Comparison between good and bad quality hot stamped structures.....	40
Table 11. Samples selected for scratch testing	41
Table 12. Scratch views for adhesive A1 at rod diameter 14µm at 106°C.....	41
Table 13. Scratch views for adhesive A2 at rod diameter 14µm at 106°C.....	43
Table 14. Scratch views for adhesive A1 at rod diameter 24µm at 60°C, 73°C and 90°C	44
Table 15. Scratch views for adhesive A2 at rod diameter 24µm at 106°C.....	46
Table 16. Scratch views for adhesive A1 at rod diameter 50µm at 73°C and 90°C.....	48
Table 17. Scratch views for adhesive A2 at rod diameter 50µm at 90°C and 100°C.....	49
Table 18. Scratch views for adhesive A4 at rod diameter 50µm at 106°C.....	51

Introduction

Multilayered structures are an integral part of every product produced out there, be it in the form of coatings or thin films, it is nearly impossible to imagine a product without multiple layers. With the advancement of technology, it is possible to produce multilayer structures from non-melt extrudable polymers and non-polymer materials like aluminum foil which is widely used in hologram technologies for product and document protection (1). These multiple layers are used for a distinctive variety of purposes, be it protective or functional. Irrespective of the purpose they are serving; their efficient adhesion to the substrate material is of foremost importance. However, in case of metallic substrate, these films are applied in the form of precursors and the strength of adhesion is significantly large due to the adsorption at the substrate surface (2). In order to achieve good adhesion between multilayer polymeric periodical structures and the adhesive layer itself, requires numerous iterations to select the optimum thickness of adhesive layer and hot stamping process regimes (mainly temperature, T and pressure, P) (3).

From the standpoint of industrial engineering, the quality of adhesion is most desirable which is directly dependent on its strength. And to evaluate this, several methods are available, for example, scratch test, indentation test, cross-cut method, etc. but the most promising method for such testing is scratch test and thereby observing the scratch imprints on the sample under the optical microscope in order to get a fair view of the results. However, adhesion bonding is not an individual mechanism but a combination of mechanisms.

This report aims to incorporate a deeper understanding by reviewing adhesion process, morphology of multilayered structures, thin layer formation methods, and to evaluate the quality of hot stamped periodic structures in dependence of adhesive layer nature and thickness.

The following tasks were performed to carry out this research:

4. To evaluate the influence of adhesive layer formation regimes on adhesive layer thickness;
5. To evaluate scratch resistance of adhesive layer vs adhesive layer formation regimes;
6. To evaluate quality of hot stamped structures in dependence of adhesive layer nature and hot stamping regimes.

1. Review of Literature

1.1. Background

The term adhesion is gaining tremendous attention these days because of its innumerable applications in almost everything being fabricated out there. Adhesion does not hold a definite syntax, many scientists and researchers proposed various theories that satisfies one or the other case. Broadly speaking, there are two types of adhesion bonding, first one is structural and the second one is non-structural. The first one is meant for substrates subjected to high loading condition and therefore the adhesive plays an important role in stress distribution without breaking its own structure while the latter one is supposed to hold low density materials in place. However, that's not always as it seems when some specific adhesives are used for certain applications which violates the aforementioned classification (2).

With the fast growing development in science and technology, the living organisms are no exception in showing incredible evolution in order to adapt to the changing environment. One such evolution is observed that certain species of animals have developed strong capability to adhere to different kind of surfaces, for example mosquitoes, water striders, gecko, tree frogs etc. Moreover, there is one such creature which exist in nature and possess this outstanding ability of adhesion, around 200 to 300 times of its own weight, abalone (4). Before Lia et al. addressed about this creature, underwater adhesion was considered highly complex phenomenon as it was greatly affected by the presence of water and might diminish various bonds strength. So they developed their own test equipments to evaluate shear and normal strength of abalone both under water and out of water on various contact surfaces and the results were astonishing. The adhesion strength in abalone surpassed adhesion capability of other creatures with almost three times and that the normal adhesion strength was higher than the shear adhesion due to presence of a mucus membrane. It was an interesting, yet not very vastly explored dimension.

This case study is primarily based on coating of adhesives and hot stamping of periodical structures, thus forms a need to understand surface chemistry, which profoundly describes wetting phenomenon resulting from mutual attractions between adhesive molecules as well as intramolecular interactions between adhesive and the substrate surface. It is the relative interactions of these molecules that determine adhesion performance parameters (5). Satas, described in his findings that rheology, the science of flow and deformation, also plays significant role as the viscosity changes during coating and stamping. A good adhesion necessarily requires right surface chemistry. Thus, in this experiment, various film formation defects and bubble formation are also recorded and based on the comparison of adhesion quality of different samples, the optimum selection is done.

1.2. Theories of Adhesion

The nature of adhesion bond essentially depends on the scale of interaction between adherend and the adhesive. An adhesive is any material applied to a surface of substrate (adherend), used to join them permanently. In general, adhesion is an interfacial phenomenon which takes place between two bodies in close contact. As a matter of fact, adhesion mechanism can be explained by combination of different theories for example, mechanical interlocking theory, electrostatic theory, diffusion theory, wettability, chemical bonding, van der waal theory, etc. Depending on the scope of interaction (i.e., molecular, atomic or macroscopic) between adhesive and adherend, and the morphology of adhesive layer (water-based or solvent-based) itself, the quality can be improved in a progressive manner.

In a recent study conducted by Yao et al., the interfacial properties between carbon fibers (CF) and polycarbonates (PC) were enhanced by pre-coating of PC resins onto the surface of fibers, followed by heating of the composition to make sure that resins are evenly coated over the surface. To test the interfacial interaction of CF and the coating, the adsorbed resins were washed away by aid of a solvent, thus it was noted that interfacial adhesion was dependent on the coating thickness as well as interactions in fiber matrix. For lower coating thickness (of order $<0.15\ \mu\text{m}$), it was observed that PC was not properly impregnated into the CF bundles, therefore, lead to poor interfacial and mechanical properties while in case of higher thickness (from $0.15\ \mu\text{m}$ to $0.32\ \mu\text{m}$), the impregnation was better and after hot pressing, the bonding became even more strong. Both shear strength and mechanical properties were significantly improved by this process (6).

Hwang et al. conducted a study to analyse hydrophobic interaction based adhesion of *Pseudomonas putida* NCIB 9816-4, a type of soil bacteria, using extended DLVO (Derjaguin-Landau-Verwey-Overbeek) theory. Since the soil particles are non-homogenous in nature, it was difficult to define physico-chemical properties such as contact angle, therefore, they used silanized silica gel as the sample soil which had more hydrophobicity than the normal gel. In this study, they evaluated surface and interfacial Gibbs energy parameters by using contact angles and zeta potentials of microorganisms. It was found that Lewis acid-base interaction was far greater than van der waal and electrostatic attractions (7).

Apart from these traditional theories there exist some advanced theories like DMT, DLVO, XDLVO etc. which broadens the extent of interactive attractions that act outside the actual contact area of adhesive and substrate.

According to **mechanical theory** (2), the adhesive enters the pores or irregularities on the substrate surface and displaces the trapped air in those voids thus increasing the contact surface area for adhesion. It was concluded that abraded surfaces are favorable sites for adhesive bonding. However, research reveals that there are naturally occurring phenomenon that shows excellent adhesive bonding between smooth surfaces, for example, the peeling model.

It is a matter of debate that which factor is truly responsible for good adhesive strength, i.e., mechanical interlocking or the increased contact surface area. Furthermore, there are evidences of data that supports the bond strength and durability due to surface roughness while some evidences prove that increasing the roughness lowers the strength of bonding (8).

It is also observed that electrostatic force acts between adhesive and the adherend when electron transfer takes place between the duo, thus inducing a strong electrostatic force of bonding. This theory is called **electrostatic theory**. An example of such bonding is a metal-polymer adhesion system. While a metallic system possesses high bond strength, a non-metallic system on the other hand shows weak signs of electrostatic mechanism (9).

When both adhesive and the adherend are polymers, then **diffusion theory** comes into play, which states that particles of adherend and adhesive diffuse together to form adhesion. The nature of bond depends on the bonding conditions as well as the material. Generally, the bond will be stronger when both materials have comparable solubility and the diffusion is taking place at temperature above the melting point of the substrate while lower strengths are observed in case of diffusion under low temperatures. For example, adhesion of polypropylene (melting point $175\ ^\circ\text{C}$) and butyl rubber.

In addition to these traditional theories, some recent theories have been put forward, like **chemical theory**. This theory states that adhesion bond is formed by the aid of chemical forces of the substrate surface. Depending on the chemical composition of the interfaces, the bonds are categorized as van der waal forces ($\text{CF}_3\text{H} - \text{CF}_3\text{H}$), hydrogen bond ($\text{H} - \text{H}$), covalent bond ($\text{C} - \text{C}$) and ionic bond ($\text{Na}^+ - \text{Cl}^-$) in the increasing energy order. The interactions at the interface in these bonds is a result of information shared by above mentioned theories (10).

Apart from this, when adhesive molecules achieve maximum contact with the substrate surface by a phenomenon called **wetting**, surface forces are developed causing adhesion. This type of adhesion is explained under **wetting theory**. Here, the bonding is formed by molecular force of attraction and the strength of bond is severely low in comparison to aforementioned adhesion mechanisms. In order to achieve good bond strength, the adhesive should completely wet the substrate, that means, it should have lower surface tension than that of substrate surface (11).

Recently, a new theory of adhesion has been discovered called as **acid-base theory** which is nothing but an extension of chemical theory. This theory was originally proposed by G. N. Lewis in 1938, which said an acid can accept a pair of electrons while a base can donate the pair. Considering this concept, acid-base theory was formulated, which states that adhesion is generated by polar attraction between Lewis acids and bases at the junction (12).

1.3. Multilayered structures

Using a combination of these theories, Prudnikov et al. presented an experimental overview about how introducing ultra **thin multi layers** of platinum on the magnetic substrate can significantly change anisotropic orientation and this, in turn, increases the magnetoresistance of these structures. These ultra-thin layers of magnetic materials are highly sensitive towards anisotropy generated by crystal field of non-magnetic substrates and their behavior were used to determine anisotropic characteristics by virtue of variable dimensions and temperatures.

In order to understand interface morphology, and interdiffusion of **multilayers** of two different materials, namely, Al (Aluminum) and Ni (Nickel), Wang et al. (2019) used TEM (transmission electron microscopy) and APT (atom probe topography) to evaluate assymetric atomic diffusion and phase growth at interfaces of Ni/Al over the substrate of Al-Ni/Ni-Al interchangeably. The study revealed that some Al atoms were able to penetrate in the Ni-Al substrate and forms nanostructured multilayers along with Ni, thus leading to spontaneous and rapid phase transformation (13).

A similar study conducted by Tang et al. (2019) revealed how dual alloy joint microstructures interface behaves under compressive deformation. They used TiAl/Ti₂AlNb joint and a typical Arrhenius type constitutive model to analyze the system under hot deformation. During the experiment, a fascinating phenomenon called dislocation creep was observed. The occurrence was accompanied by O-phase decomposition and precipitation in the base metal. Moreover, one more phenomenon occurred at the interface, but the critical point of consideration is the decomposition in the base metal due to deformation at high (around 1000 °C) temperatures.

In recent study, an efficient method of producing multilayered substrates for power applications was composed by Hilna et al. (2019). The method is based on co-firing of material (Cu) on the substrate using TPC (thick printed copper) technology. The study showed that electro-mechanical **multilayer structures** can be produced efficiently by co-firing. This was another successful example of using

TPC technology for creating multilayer structures. There can be several crossovers depending on the application, thus the scope of efficient production of these structures is incredibly high.

In 2017, Liu et al. used vacuum diffusion bonding for joining super laminated composite (Ni/NiCr) with Ti-6Al-4V. The results showed that bonding time had drastic effect on the microstructure at the interface of similar constituent materials. Some of the layers transformed from serrate to straight, some joints fractured at the interface and emitted a dependence on the bond time from increasing to decreasing and finally towards plastic deformation. So, the timing must be optimized in order to get the best bonding result.

Assari and Eghbali (2019) also synthesized **multilayered composite** of Al and Ti using hot press and hot rolling. In this study, intermetallic compounds were observed at the interface and thickness of structure increased with increase in annealing time and temperatures. Al, being the dominant diffusing element had voids on its layer because of diffusion discrepancy between Al and Ti elements. The ultimate strength was altered by hot pressing the specimen twice, because strain hardening also increased. An important aspect to be noted here is that if the inter-crystalline structure of the adjoining materials ruptures, then the interface will be fractured. So, hardening must be such that it should not be too hard (14).

In 2015, Khoramkhorshid and his team used ARB (accumulative roll bonding) to produce glass powder reinforced Al based composite. It took several ARB cycles to uniformly distribute glass particles in the Al matrix but the results were super good. The composite was characterized by excellent metallic bonding, increased microhardness, tensile strength and various other mechanical properties in comparison to individual matrix properties (15).

Another study, conducted by Rao et al. (2018) depicted how a thin interlayer of Cu improved the bonding strength and proper adhesion of two refractory metals, 93W and Mo1. The interesting point is, bonding took place at comparably low temperatures, using plasma activated sintering method. The constituent elements in the alloys readily diffused with the adhesive Cu layer, thus resulting in higher strength at both interfaces (16).

According to Cammarata, a thin film on the substrate is often deposited under stress. Mostly it is desirable to have stresses but sometimes it can catastrophic causing the material to crack or may lead to de-adhesion. The main microstructural feature of thin films is that the surfaces possess huge density in comparison to conventional complicated materials. And these surfaces have considerable effect on the mechanical behaviour of thin films and their possessed stresses. When the lattice microstructure matching is maximum between film and substrate surface, it will result in defect-free interface, however, if the duo have difference in equilibrium lattice spacing, and substrate has a thicker profile, then the film has to be strained according to the substrate structure so as to match with the atomic structure of the substrate. Therefore, an epitaxial relationship between thin films and substrate was called as mandatory (17).

1.4. Water-based adhesives and adhesive testing

Santos et al., (2016) formulated a **water-based adhesive** from a tree bark, in order to join lignocellulosic surfaces, wood and cork. First, they extracted cork in aqueous state by liquefaction of biomass (in this case, wood/cork) under the presence of alcoholic acid catalyst. This obtained solution is then mixed with an aliphatic compound to create an adhesive like structure. Finally, the main ingredient, i.e., cork powder is added to the structure to form stable adhesive with superior shear strength.

Soon after this, Botero, Lainez, Acosta and Martinez (2017) also conducted an experiment to produce waterborne adhesive for rubber to metal bonding. They investigated the effect of constituents of waterborne adhesive on the rubber-metal bonding through various DOE methodology. After conducting many experiments with varying conditions, and rigorous adhesion evaluation, they concluded that substances like tackifier resin, silicon dioxide and polychloroprene latex have significant influence on adhesive as well as cohesive forces.

Studies revealed that water based adhesives have both advantages as well as disadvantages over conventional solvent based adhesives despite of completely different mechanical properties among the duo. Some nanoparticles such as nanoclay (NC) have found tremendous applications in coatings in order to enhance the mechanical characteristics. Anwar et al. conducted a study in which they mixed NCs to water based coatings in an optimal percentage and thereby formulated a comparison between the mixed and non mixed compositions. For this process, NC particles were dispersed in different percentages to make the samples. Then effects of NC on mechanical properties of coatings on wood including adhesion, impact test, scratch resistance and abrasion were studied. In case of adhesion, no failure was reported at lower percentages, of the order 2%, 4% and 6% of NC while in higher concentrations (8% and 10%) poor adhesion was observed. It was then concluded that increasing the amount of NC would enhance the mechanical properties but only upto a certain level after that it starts diminishing again (18).

In order to improve adhesion strength, Li et al. (2019) conducted a study by depositing multiple nitride coatings on two different specimens one with polished steel and the other one plasma nitrocarburised. It was observed that nitrocarburizing improved the adhesion strength of the specimen as compared to the polished steel. This enhancement of tribological properties was regarded as a result of hardening of substrate surface through diffused nitrocarburized layer.

The mechanical properties and behavior of adhesive films are greatly affected by the stresses. If these stresses reach the plastic deformation limit, it can cause adhesion failure, so it is an important aspect to be considered. It should be noted that substrate materials generally inhibit higher rigidity than that of coating. In such case, the failure will occur within the coating, if system experiences external force of relatively high intensity. Consequently, cohesion failure may take place, if the adhesion at the interface exceeds the cohesion of the film. Otherwise, only adhesive failure will be observed which will cause detachment of film and the substrate (19).

It has been clearly stated in a recognised literature source, composed by K. L. Mittal (2006), written by Cammarata (2005), that surface stresses are not only function of mechanical behaviour and surface conditions but also because of the surface thermodynamic parameters. These stresses are intrinsic in nature. Although higher stresses can cause serious effects like cracking, spalling and de-adhesion but often times these stresses are desirable for thin film formation.

For example, in case of electronics where several epitaxial layers of semiconductors are required to be deposited on a single crystal substrate to obtain flawless interface of film and the substrate.

A study conducted by Rudawska et al. (2016), indicated that for steel, the type of abrasive material used plays vital role in manipulation of surface properties in comparison to changing process parameters. As altercated by Bazrafshan in 2019 who claimed surface free energy and surface characteristics for adhesion are highly dependent on the interaction between surface texture as well as the adhesive applied. But the fact is, both are true to the extent of their field of study like in the latter case, a smooth silicon specimen was used, which justifies their research (20).

Cammarata (2005), further described that main microstructural feature of thin films is that the surfaces possess huge density in comparison to conventional complicated materials. And these surfaces have considerable effect on the mechanical behaviour of thin films and their possessed stresses. When the lattice microstructure matching is maximum between film and substrate surface, it will result in defect-free interface, however, if the duo have difference in equilibrium lattice spacing, and substrate has a thicker profile, then the film has to be strained according to the substrate structure so as to match with the atomic structure of the substrate.

A similar experiment conducted by Munagala, Imbriglio and Chromik (2019) claimed that microstructure of splats in cold spraying immensely affect the adhesion strength of sprayed coatings. To demonstrate this, they used two types of powders, one is with spherical particles having martensitic microstructure and the other one irregular particles having equiaxed microstructure. Using **splat adhesion** test, it was confirmed that irregular morphology of irregular powder allowed more deposition on the adherend but interestingly, the post spray structure was distorted. While in case of spherical powder, the adhesion strength was lower but the retention of structure was superior.

According to a recent research on conversion coating by Xu, Wang and Gu, (2019) it was proved that deposition of conversion coating of Ce on Al foil effectively improved the adhesion strength as well as hydrophobicity of the foil. The purpose of this research resolved a packaging solution for lithium ion batteries. The coating quality was evaluated using **T-peeling test**.

In early 2010s, a modified **scratch test** was introduced by Sander, Tremmel and Wartzack (2011) for both hard and soft coatings. They suggested to use indenter balls made of hardened steel for conducting the test. Using different diameter of balls, helped to analyze tribological and mechanical behavior of both the material and the interface. The results also displayed that small diameter ball indenters are way better than the sharp diamond edged one (21).

Furthermore, to evaluate the bonding strength at the interface, it is necessary to determine the maximum stress that can be attained at the interface. If sufficient energy is provided at the interface, then it can be expressed as the work of adhesion, which is equivalent to the product of adhesion strength and the distance between separated surfaces of coating and substrate after detachment. Mathematically, it gives us the stress value. As a matter of fact, the mechanical damage occurs due to scratches or impact loading on the coating. This causes deterioration of the coating and may lead to loss of adhesion if the intensity of load is more than the tolerance level of the film.

1.5. Adhesion test methods

1.5.1. Cross-cut method

This method is based on the estimation of amount of separation of adhesive from the substrate using a cross-cut tool. Firstly, a cross-cut is made on the coating and loose parts are brushed off. Then the detached flakes are obtained on an adhesive tape by sticking on the cross-cut section. These observations are classified according to ISO and depending on the classification, the percentage of flaking is recorded. Classification '0' indicates the perfect adhesion condition whereas all higher ones are regarded as poor adhesion (as indicated in Fig. 1).

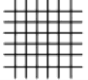
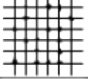
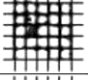
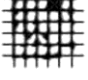

Score	Appearance of surface of cross-cut area from which flaking has occurred
0	
1	
2	
3	
4	
5	—

Fig. 1. Classification of cross-cut (22)

1.5.2. Indentation debonding

This method is used when the substrate material is virtually undeformable in nature and most of the deformation occurs in the film and thereby, causes certain debonding at the interface. The method uses a needlelike indenter which is pressed perpendicularly into the surface of the coating (Fig. 2). In this situation, a peeling moment can be calculated, which serves as a measure of film's capacity to withstand delamination near the indentation site.

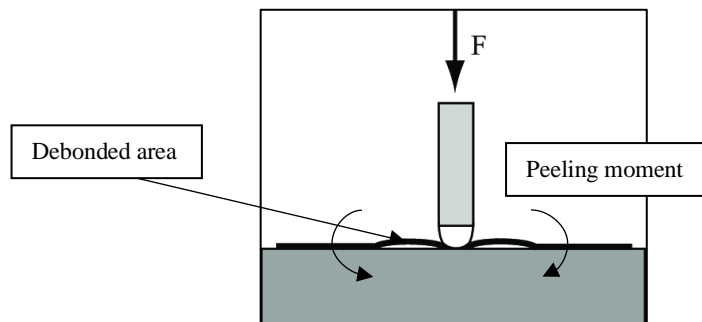


Fig. 2. Indentation debonding (23)

In order to calculate the best result, taking into account the boundary conditions at the interface, it is recommended to use a 60° angle cone indenter. The advantage of this method is that it yields the values for bond strength as well as gives information about the durability of adhesion between substrate and the adhesive under specific loading conditions.

1.5.3. Scratch test

In this method, adhesion of the coating as well as its scratch resistance can be measured. As shown in Fig. 3, a scratch stylus loaded with specified load is drawn across the film surface at a constant speed. The scratch is then observed through perceptible relationship between the applied load and the intensity of penetration, which eventually causes peeling off the coating.

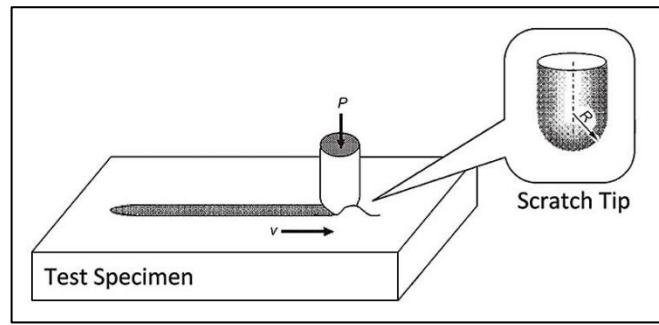


Fig. 3. Scratch test set-up (23)

Here, hardness (H) can be calculated as:

$$H = \frac{4P}{\pi B^2}$$

And operating force (F) as:

$$F = \frac{4P}{\pi B \sqrt{D^2 - B^2}}$$

Where,

$P =$ Probe loading

$B =$ Width of contact area, and

$D =$ Diameter of probe

Once these values are obtained, a deeper insight can be generated by supplementing additional information about the scratch topography using profile projectors or electron microscopes. Furthermore, the type of film failure can also be determined when subjected to scratch loading.

Browning et al., in their experiment utilized a quantitative method to explore scratch resistance of polymeric coatings. The sample was composed of steel substrate coated with acrylic polymers. In their testing, they used progressive loads and thus determined critical failure load as well as type of coating failures such as delamination, cracking and buckling. Optical microscopy and scanning electron microscopy were used as investigating technologies to characterize the coating failure. Since the experiment was based under the guidelines of ASTM D7027-05, so the evaluation was mainly focused on coating ductility and thickness. The results showed that ductile coatings undergo lesser damage in comparison to brittle coatings and further, in terms of thickness, there exist a critical thickness value which can withstand coating damage. In other words, there is a certain thickness value upto which the effect of failure modes (delamination, buckling or cracking) increases with thickness but after that, it starts falling off. This study showed that coatings can be optimized to save cost and enhance life (24).

There are many possibilities for practical combinations for adhesion test systems. Although, the aforementioned methods are quite reliable and accurate for this project but still it is nevertheless predetermined which method can deliver the perfect result, so any alterations are expected while dealing with the pragmatic situation during the testing.

2. Experimental part

The experimental section of this study is about coating of adhesive layers on periodical polymeric substrate and then inspecting adhesive strength by aid of scratch test and thus defining dependence of adhesion on the coating thickness. Proceeding further, the next step is about performing hot stamping on the coated samples, and thereby evaluating the dependence/behaviour of adhesive with respect to the hot stamping regimes using scratch tests.

2.1. Materials

2.1.1. Polymeric substrate

Fig. 4 represents typical structure of aluminium coated multilayer film with thickness, $h = 19\mu\text{m}$. For this study, the substrate dimension was taken of dimensions $280 \times 200 \text{ mm}$.

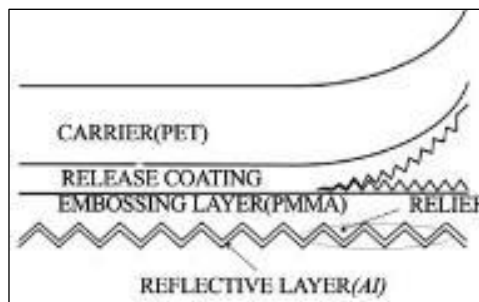


Fig. 4. Polymeric Foil Structure

2.1.2. Adhesives

To prepare samples, four different adhesives were selected in total out of which three were water-based (S35.3197 and S35.3213 (Nolax, Switzerland), OPU746 (Lotto, Germany)) labelled as A1, A2 and A3 respectively and fourth one was solvent based TC-03 (Centro Grafico DG S.p.A, Italy), labelled as A4, the details are mentioned in Table 1.

Table 1. Adhesives details

Label	Commercial name	Producer	Nature	Concentration, %	Viscosity, mPas at $T=20^{\circ}\text{C}$, $w=140$ rpm)
A1	Nolax S35.3197	Nolax, Switzerland	Water born	52	64
A2	Lotto OPU746	Lotto	Water born	86	-
A3	Nolax S35.3213	Nolax, Switzerland	Water born	40	35
A4	Solvent Based	Centro Grafico DG S.P.A, Italy	Solvent based	10	13

2.2. Adhesive layer formation

All adhesives were consecutively applied on the polymeric substrate by means of a pipette tube and then coated on individual multilayer polymer sheets by K control coater machine (manufactured by RK printcoat instruments) as shown in Fig. 5. The machine speed and pressure were fixed throughout

the experiment so as to maintain the uniformity among the samples. For this study, various rods with different wire diameters 4 μ m, 14 μ m, 24 μ m, 50 μ m and 80 μ m labelled as D1, D2, D3, D4 and D5 respectively were used. The adhesives were applied in front of the meter bars in continuous line form and then the machine pushed the rod, spreading adhesive on the substrate sheets, at constant speed and pressure.



Fig. 5. K printing proofer

After every coating, the bars and the vacuum bed were thoroughly cleaned using ethanol. The samples formed by this combination were labelled and are marked with (**) in Table 2. The setup was free from any dust or debris and the foil used was radically flat, i.e., without any bends, scratches or crease marks. The adhesive layer covered almost 80% of the surface area, which was more than adequate to conduct this study.

Table 2. Samples made by combination of adhesives and coating thickness

Adhesive	D1	D2	D3	D4	D5
A1	**	**	**	**	∞
A2	**	**	**	**	∞
A3	∞	∞	**	**	**
A4	**	**	**	**	∞

An important point to be noted is that A3 had remarkably low viscosity as compared to other adhesives, due to which it was not feasible to make samples at lower rod wire diameter (D1 and D2), therefore, only higher diameters were used for this case. Similarly, it was practically impossible to fabricate samples marked with ∞ using this method, so these samples were disregarded. All other prepregs were successfully produced under similar conditions, same process and on the same day, so as to avoid any kind of variation in the procedure. After fabricating, all prepregs were left undisturbed in a dust free environment for 24 hours for drying.

2.3. Adhesive layer thickness measuring

After the samples were dried up, coating thickness was then measured using Coating Thickness tester, CEM DT-156 (as shown in Fig. 6). The gauge was designed for non-destructive testing and worked on the principle of eddy current for measurement on non-ferrous or Al substrates (as in this case). Before measuring the coating thickness, the primary task was to calibrate the gauge since it was stated

that there exist a general tolerance of $\pm 3\% + 1.5\mu\text{m}$ (for $< 850\mu\text{m}$ coating thickness), so in order to minimise the error, several readings were taken on the Al zero calibration plate, which was provided with the instrument, to set the reference point for measurement. After calibration, to check the actual reading error of the gauge, the thickness of zero test plates were measured. As a result, the error was as low as $0.1\mu\text{m}$ which was acceptable for this study.



Fig. 6. Coating thickness tester

Once setup was completed, the thickness of each sample was measured both with coating and without coating by taking several measurements at different locations in both cases. Then the averages were calculated separately for coated and non-coated surfaces. Finally, the difference of these averages resulted in the coating thickness and thus comparative analysis was done between adhesive layer thickness and the thickness applied.

2.4. Optical microscopy

After measuring layer thickness, further testing was done to represent the surface texture of the adhesive layer. In other words, how the adhesive particles are arranged over the substrate surface. As the name suggests, a fluorescent optical microscope (with fluorescence accessory Magnification $\times 1500$ and measurable specimen dimension upto 100 mm in diameter and 50 mm in height) was used for this step (Fig. 7).



Fig. 7. Optical Microscope

To study the microscopic structure of dried up adhesives, small portions (around 15mm x 30mm) were cut from the prepared samples, laid on individual glass slides and observed under the microscope with appropriate magnification factor, depending on the clarity of visual images.

2.5. Scratch Testing

The setup for this test consists of an indenter with round tip, two additional weights measuring 2g and 5g along with scratch testing machine. The test specimen were made exactly in the same way as in step 2.4. After the preparation, the specimen was fixed on the machine bed so as to avoid any unwanted motion and the indenter is placed at the starting position of the scratch on the specimen. Initially, there was no load variation, only weight of stylus. The indenter was set to move horizontally, at constant speed, on the surface (Fig. 8) for a certain length by the aid of scratch testing software. Since this test was conducted to study the adhesive strength, so for better analytics five different weights 309.89mN, 290.28mN, 260.86mN, 329.5mN and 358.92mN were used and corresponding five scratches per sample were labelled as S1, S2, S3, S4 and S5 respectively. In all five scratches, the speed (v) of the motion of indenter is kept constant for sake of uniformity.

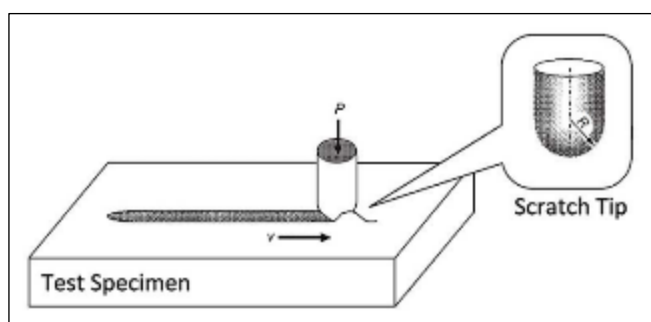


Fig. 8. Scratch test setup

This typical setup for scratch test is quite common for the performance evaluation of adhesives. In this experiment, the indenter drags across the adhesive layer in straight line with different constant loading conditions, as mentioned above. The penetration of indenter depends on the loading and thus defines the load bearing capability of the adhesive. Typically, there are three kinds of failures in scratch test: plastic, elastic and fracture (25).

2.6. Groove Width determination

After scratch test, samples were inspected under optical microscope to obtain clear images of grooves formed by indenter.

Once the images were obtained, the groove widths were measured by using *ImageJ 1.x* software (created by Wayne S Rasband, 2012).

2.7. Hot stamping procedure

The samples for this part were created by cutting off appropriate length of coated polymer sheet to fit on the hot stamping machine bed of size 10cm x 10cm. This step is carried out using hot stamping machine as shown in Fig. 9. The substrate used for this process was ordinary paper and the stamps were obtained at different temperatures 60°, 73°, 90°, 106° and 113°C, with constant press load (18N) for duration $t = 1s$.

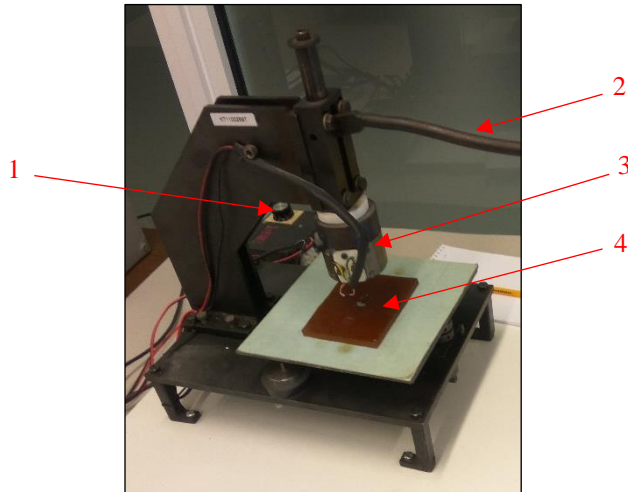


Fig. 9. Hot stamping machine (1 - Temperature regulator; 2 - Press Lever; 3 - Stamping Die; 4 - Stamping Bed)

The coated sheets were placed on top of substrate such that periodical structures were printed on the substrate. Then the lever was pushed downwards under a load of 18N on the sample, kept below, for one second. The diameter of circular heating head was $d = 19\text{mm}$.

2.8. Hot stamping quality evaluation

After obtaining the stamps, all samples were scanned to visualize the images of periodical stamps using office image scanner. Thereafter, film coefficient was obtained using the following relation:

$$\text{Film coeff. } (\epsilon) = \frac{\text{Surface area of sample stamp}}{\text{Ideal Surface area}}$$

2.9. Adhesion Evaluation

To study the strength of adhesion of holographic periodical structures, scratch test was conducted in the same manner as in step 2.5 with same constant loads with an additional one, weighing 24.6g and the corresponding scratch was labelled as S6. Then the scratch width is determined as in step 2.6.

3. Results and discussions

3.1. Influence of adhesive nature on adhesive layer thickness

The viscosity of adhesives highly influence layer thickness. For instance, samples with higher viscous coefficient were likely to adhere to the substrate better than adhesives with lower viscosity. Moreover, lesser the viscosity, more difficult was to obtain good adhesion and therefore, unusual pattern was observed in case of solvent based adhesive. Fig. 10 indicates adhesive layer thickness dependence on coating rod diameter used for deposition.

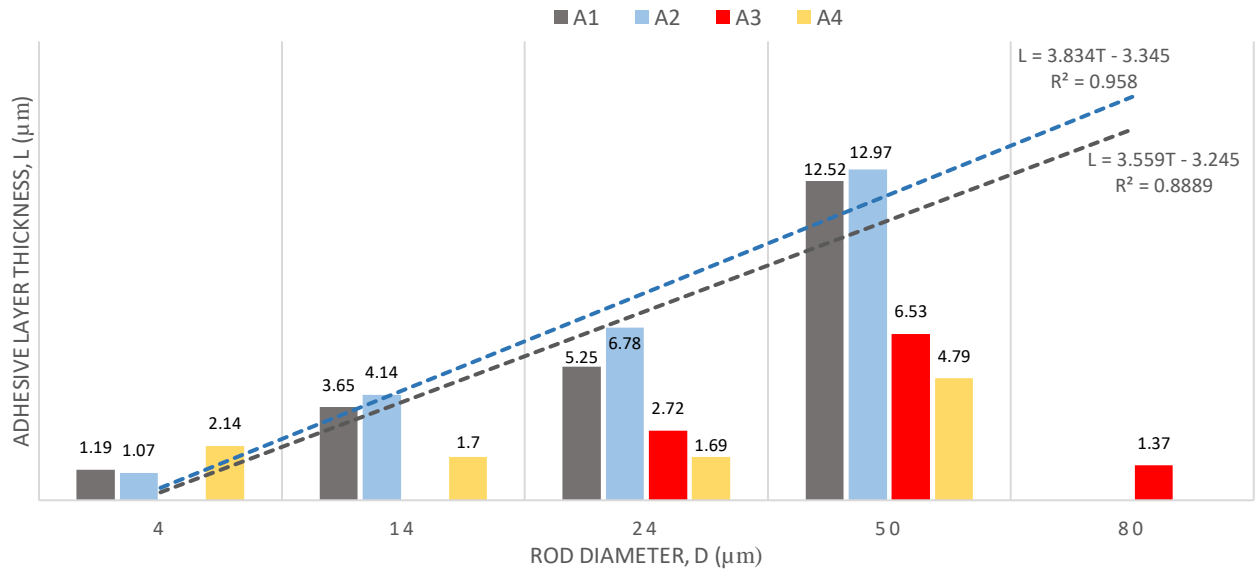


Fig. 10. Graph between rod diameter vs adhesive layer thickness

The graph indicates that A1 and A2 follows linear dependence of adhesive layer thickness with rod wire diameter with R^2 factors of 0.958 and 0.889 respectively which explains that these adhesives have comparatively high viscosity and good interlayer adhesion capability. While the other two, with lower viscosity show unusual patterns. Adhesive 3 (A3) has very low coefficient of determination value because the thickness of layer first increases from 24μm to 50μm and then decreases drastically at 80μm. This proves that this adhesive is highly sensitive to the coating thickness and may lose adhesive strength after a certain threshold point. There is no mathematical relation between adhesive layer and the wire diameter that satisfies all three observations. So, it can be stated that this adhesive is suitable to coat at diameters within close tolerance to 50μm.

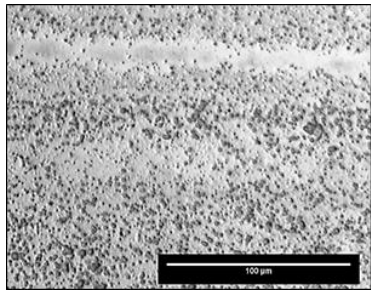
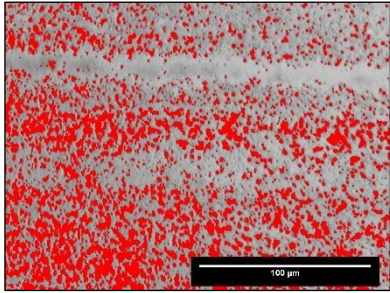
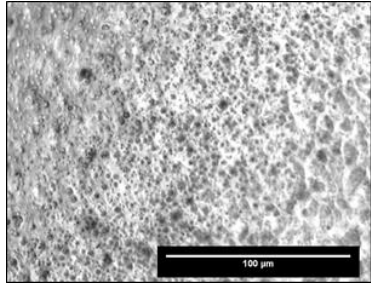
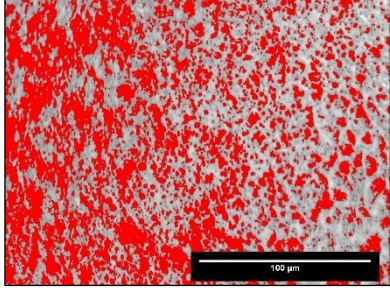
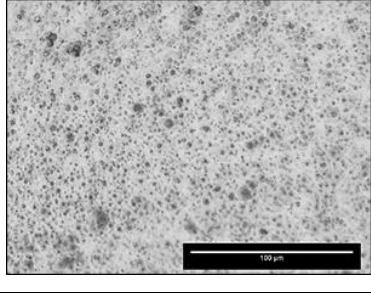
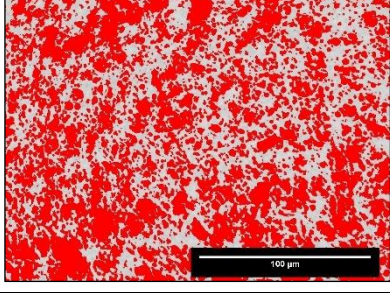
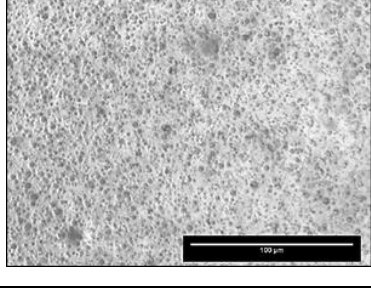
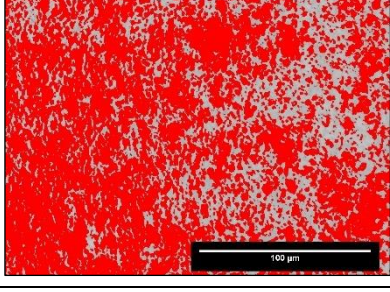
Adhesive 4 (A4), however, shows even more complicated behaviour than A3. At 4μm, it represents good retention as compared to A1 and A2 but gradually ceases to maintain the interlayer adhesion till 24μm, which implies presence of more solvent particles in the overall adhesive concentration, due to which more particles evaporated from the layer. And after a certain value again starts retaining the layer but this time significantly lesser than the other adhesives. Additionally, the regression correlation for this adhesive is significantly low, thus it can be said that this adhesive has no dependence to the rod wire thickness.

Overall, it can be seen that at 50μm all adhesives display incredibly good results however, best quality of adhesive will be evaluated based on further testing of adhesive-substrate adhesion as well as interlayer adhesion.

3.2. Evaluation of adhesive layer structure

To analyse layer structure, observed samples show certain amount of unevenness of the layer with respect to rod wire diameter. There are two images for each sample, the first one indicates actual microscopic structure while the other one shows analysis conducted by aid of ImageJ software. The area highlighted in red represents unbalanced waviness of surface and it varies with increasing thickness because more and more particles were deposited, thereby covering more surface area. Table 3 shows variation of surface area of unevenness with the rod diameter.

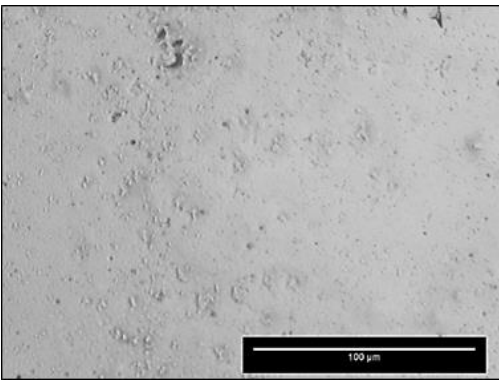
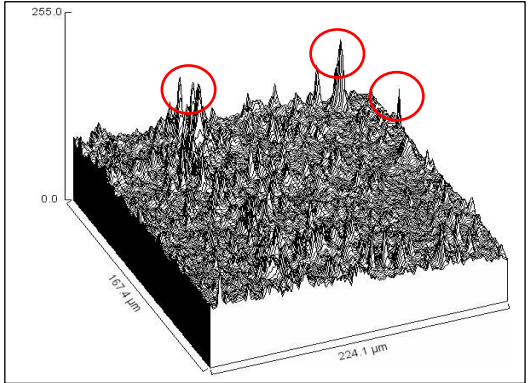
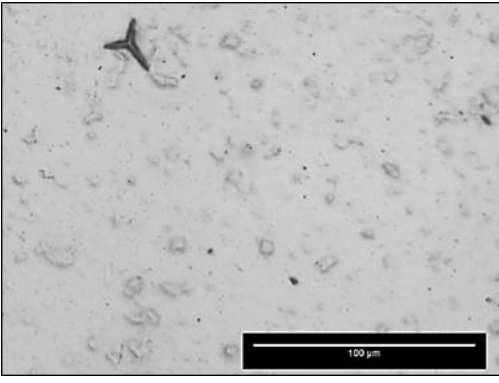
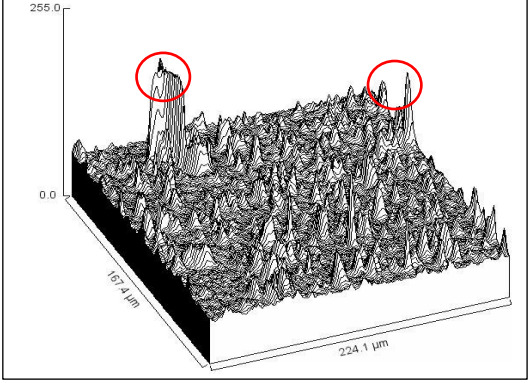
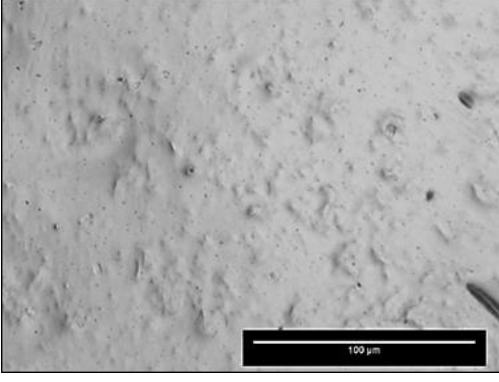
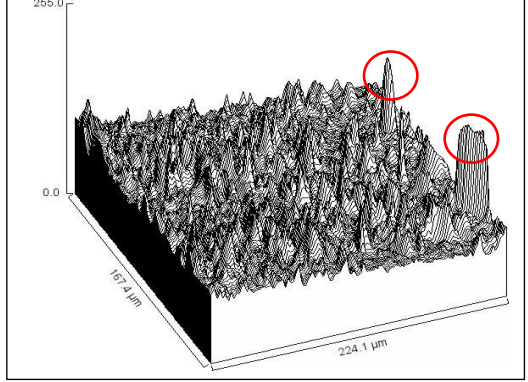
Table 3. Adhesive A1 surface analysis

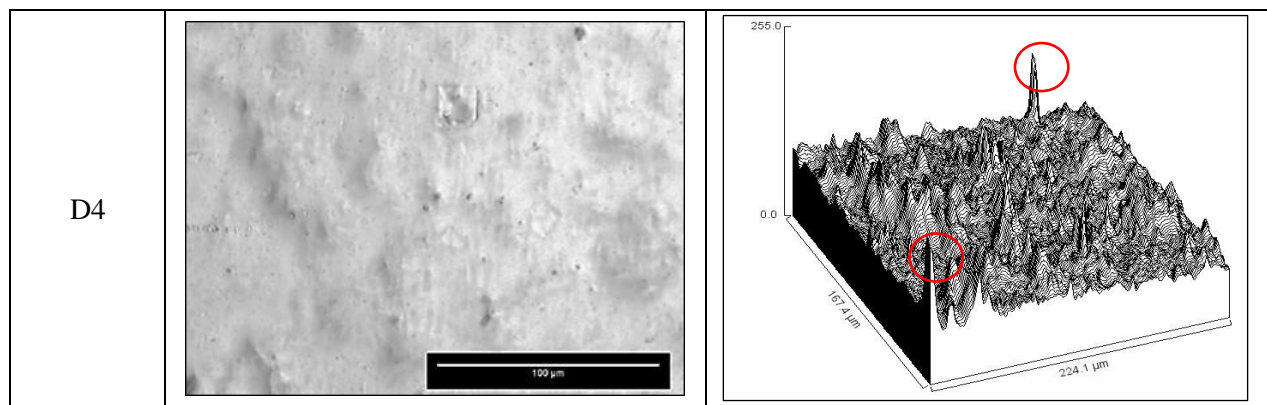
Wire Diameter	Optical microscopy	Analysed Image	Percentage amount of unevenness
D1			28.18
D2			40.64
D3			55.33
D4			67.24

As per image analysis, D1 has lowest percentage of unevenness with 28.18% of the total surface area which means that this sample has more smooth texture and this smoothness reduces with increasing wire diameter. The increasing percentage of unevenness from top to bottom confirms that layer structure is highly dependent on the rod wire diameter. Thus covering maximum surface area with 67.24% of total surface area as in case of D4.

Adhesive A2, on the other hand, has higher viscosity than A1 so for this sample, wire frame plot was used to study the surface texture because the previous method was not possible. In this case, the layers were almost homogeneous throughout the surface, however there were some higher peaks observed during the analysis which indicates irregularity over the entire layer surface. These peaks were marked with red circles in Table 4. Moreover, analysis revealed that grain structure of A2 was highly coarse, therefore, higher peaks were observed only at specific places and not on entire surface of layer. Additionally, the widths of the peaks in the graphs can be seen increasing from top to bottom which essentially indicates increasing density of adhesive deposition with increasing rod wire diameter.

Table 4. Adhesive A2 surface analysis

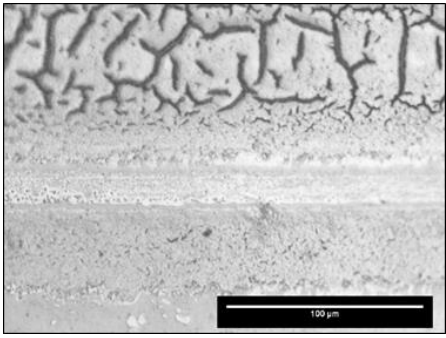
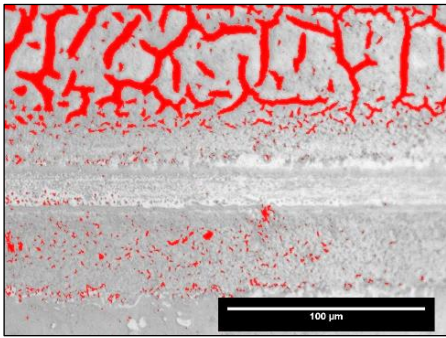
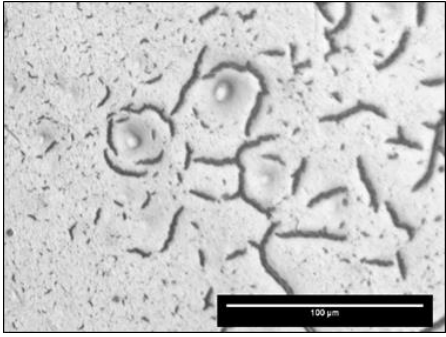
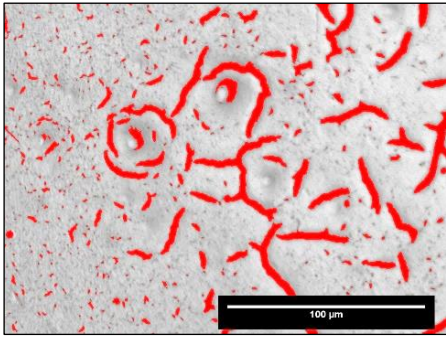
Wire Diameter	Optical microscopy	Wire frame plot
D1		
D2		
D3		

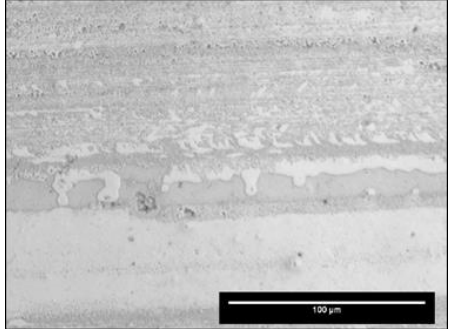
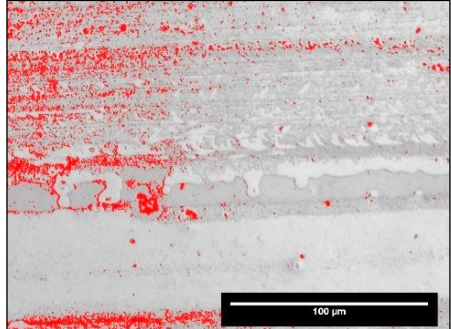


Some wider peaks were observed in case of D2 and D3, indicating cracks in the surface which might have formed due to layer contraction during the process of evaporation of moisture. Similarly, more wider peaks in case of D4, because of higher density.

Moving on to adhesive A3, the structure looks uneven with different textures all over the surface with large gaps in between. The reason behind this heterogeneous deposition pattern over the plane of layer could be low viscosity, which makes it difficult to adhere on the substrate properly. Also, high sensitivity towards surface roughness of the substrate as well as quick evaporation of high amount of organic solvents causing defective structure formation. Table 5 shows structural analysis for adhesive A3 with rod wire diameter D3, D4 and D5, since lower thickness coatings were not possible, along with percentage of voids or defected surface formed.

Table 5. Adhesive A3 surface analysis

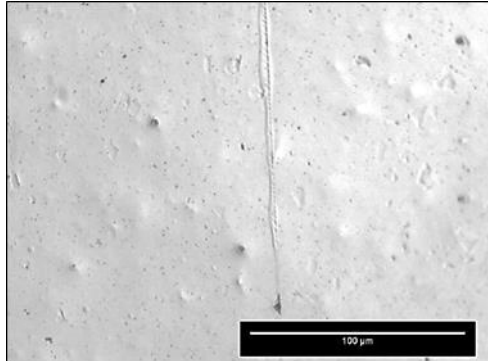
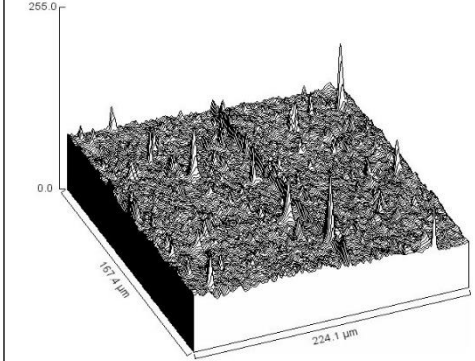
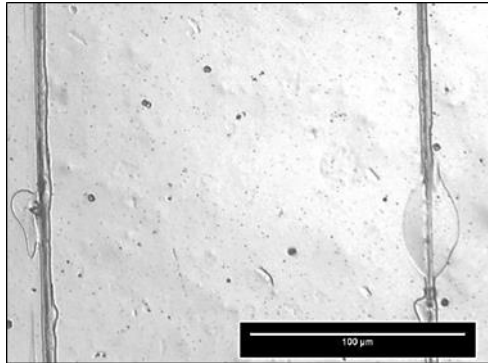
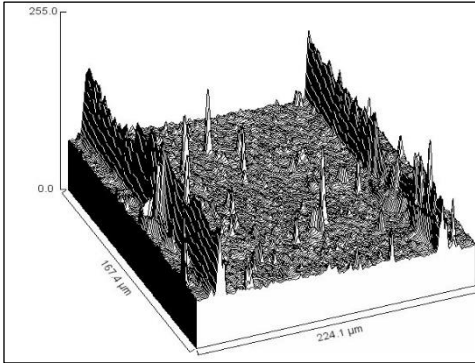
Wire Diameter	Optical microscopy	Analysed Image	Percentage of void
D3			12.62
D4			11.06

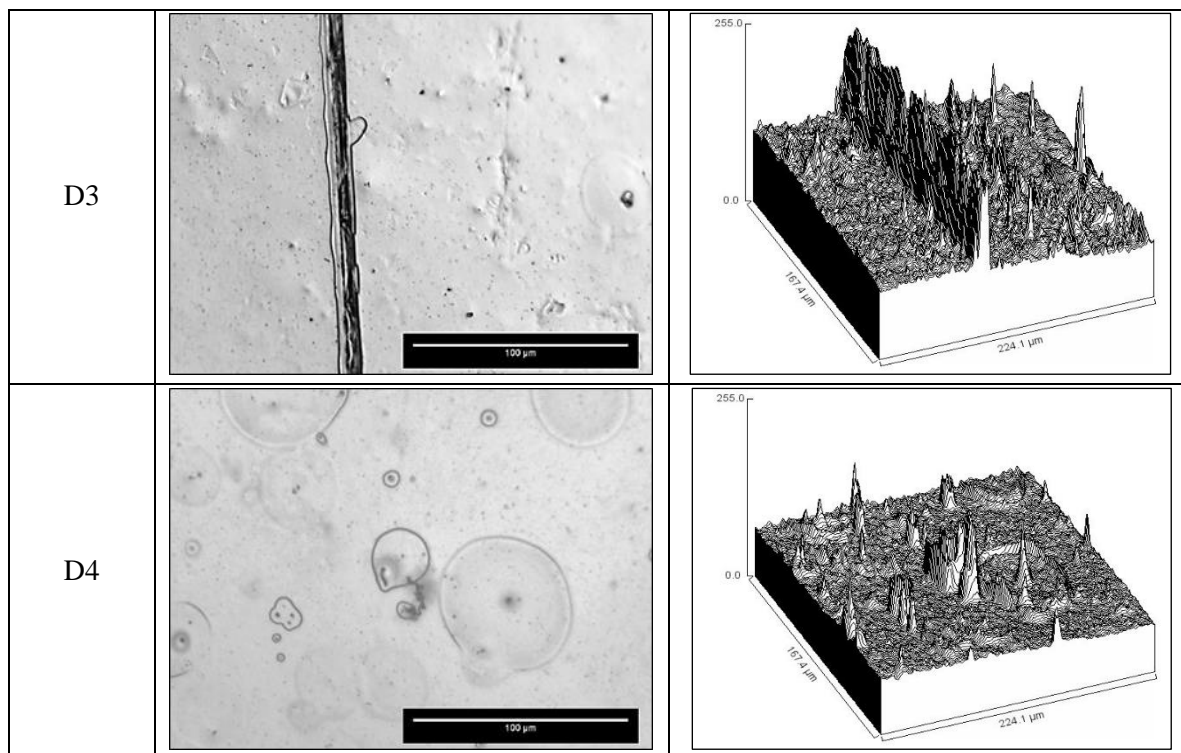
D5			6.92
----	---	--	------

The decreasing percentages from top to bottom indicate reduction in area of defected surfaces. This shows higher thickness was able to coat substrate surface more productively resulting in better adhesive layer cohesion retention.

Similar to adhesive A2, A4 also projects smooth and homogenous deposition throughout the surface accompanied by bubble like formations, which must have been formed due to the higher surface tension of solvent particles present in the adhesive. Again, in this case it was not possible to analyse the unevenness by surface area method therefore wire frame plot was used to determine surface deformation. Table 6 displays analysed images with look alike peaks over the entire surface area as in case of A2. These peaks represent areas of deformation or irregularity present on the surface. Some linings were observed in the optical microscopy which gets darker from D1 till D3 but vanishes in thickness greater than D4. The possible reason for this could be the coating rod wire which left impressions during application of lower thickness coats.

Table 6. Adhesive A4 surface analysis

Wire Diameter	Optical microscopy	Wire frame plot
D1		
D2		



From wire plots of Table 6, D1 shows least signs of deformation with minimum number of peaks, i.e., deformation and the layer looks more uniform. For D2, the deformation mainly occurred at impressions marks as discussed in previous text while remaining structure is similar to D1. In D3, there are more number of peaks in comparison to D2 which shows more layer deformation as well as more thickness than D2. The peaks can be seen wider in case of D4 because of higher wire diameter and formations of bubbles due to difference in surface tension of adhesive molecules which left recovery marks after evaporation.

Overall, it is noted that there is huge variation in structural patterns of all fifteen samples which means the selected samples would derive a good comparative analysis however, the quality of adhesion will be evaluated by measuring the scratch resistance which will be discussed further in this chapter.

3.3. Evaluation of adhesive properties between multilayer films and adhesives

Adhesive strength for thin layers can be evaluated effectively by scratch test method by using different scratch loadings. This testing determines critical load condition when the layer starts to deform or fail. When the failure takes place within layer, it means adhesion strength exceeds cohesive strength of adhesive and it becomes very difficult to evaluate the strength. However, the type of failure and groove width contributes in determination of mechanical properties of the adhesives.

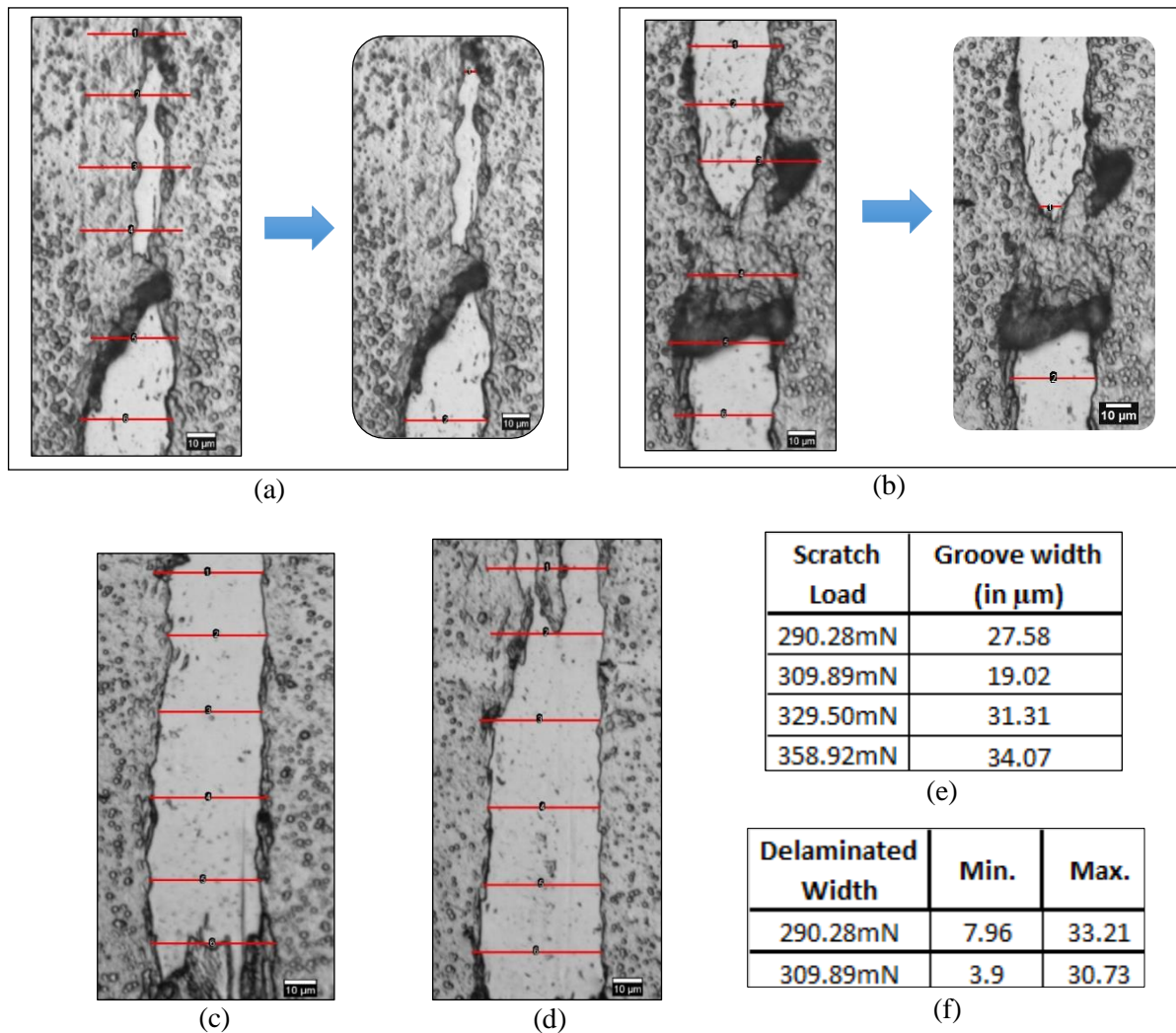


Fig. 11. Multilayer structures for sample adhesive A1 at rod diameter $4\mu\text{m}$ under scratch loads (a) – 309.89mN (b) – 290.28mN (c) – 329.5mN (d) – 358.92mN (e) – Groove width (f) – Delaminated width

As mentioned before, each scratch corresponds to specific weights of the indenter. All scratches are made in the same manner and in the same direction. For 309.89mN and 290.28mN separate results have been displayed, which represents the width of cohesive failure. 309.89mN and 290.28mN have discontinuous failure pattern which justifies lesser loading condition in comparison to 329.5mN and 358.92mN . Here, 309.89mN is the least load applied, hence there is no visual scratch obtained in this case. There are some discontinuity seen in the patterns of 329.5mN and 358.92mN which might be due to roughness of substrate surface. In Fig. 11, table (e) enlists groove widths of all scratches calculated by taking average of six values as represented by horizontal red lines while in table (f) range of distorted groove width is given. This means the adhesion failure in 309.89mN and 290.28mN lies in that limit.

In case of A1/D2, a drag impression of indenter movement was observed which caused cohesive failure on the adhesive layer for loadings 309.89mN , 329.5mN and 358.92mN while negligible effect was seen for loadings 290.28mN and 309.89mN . This sample shows higher adhesion ability in comparison to the previous sample (Fig. 12).

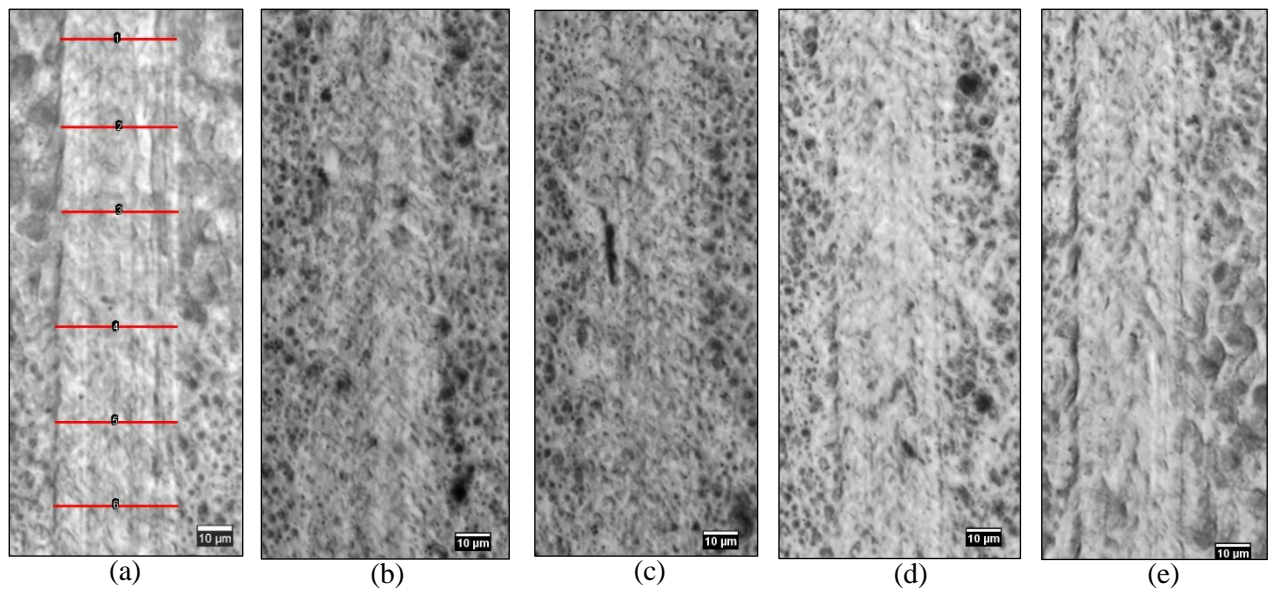


Fig. 12. Multilayer structures for sample adhesive A1 at rod diameter 14 μ m under scratch loads
 (a) – 309.89mN (b) – 290.28mN (c) – 260.86mN (d) – 329.5mN (e) – 358.92mN

The groove widths were measured in the same manner as in previous sample and the plot of observations are shown in the next subsection of this chapter.

Similarly for A1/D4, scratch pattern resembles to patterns observed in A1/D2 (Fig. 13). There is minor cohesive failure over the top surface of adhesive layer and no sign of adhesive failure. The same measurement technique is used and the plots are depicted in the next subsection.

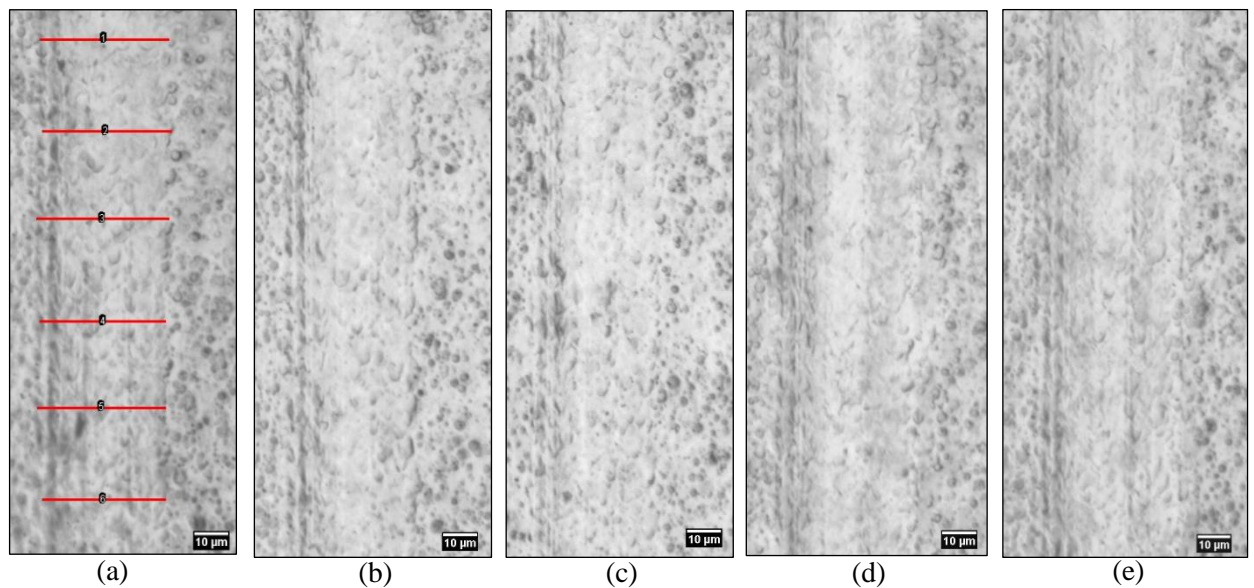


Fig. 13. Multilayer structures for sample adhesive A1 at rod diameter 50 μ m under scratch loads
 (a) – 309.89mN (b) – 290.28mN (c) – 260.86mN (d) – 329.5mN (e) – 358.92mN

In A2/D1 as shown in Fig. 14, adhesive failure can be observed in all loading conditions. Here, 309.89mN has a separate image to denote the actual adhesive failure width, using the same six value averaging measurement technique, however, the total groove width is more than that. This is because of the additional cohesive failure of the layer along the length of scratch.

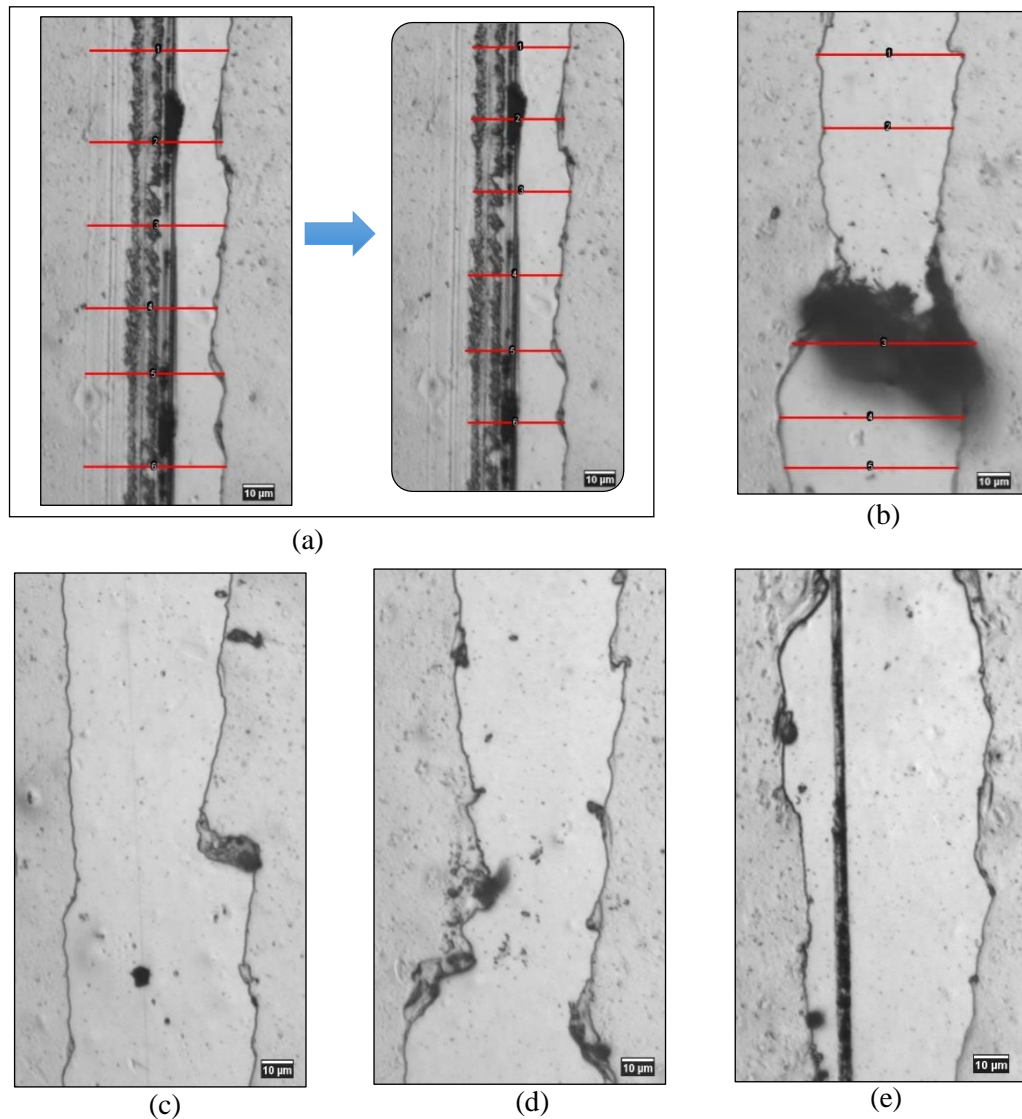


Fig. 14. Multilayer structures for sample adhesive A2 at rod diameter $4\mu\text{m}$ under scratch loads
 (a) – 309.89mN (b) – 290.28mN (c) – 260.86mN (d) – 329.5mN (e) – 358.92mN

In all other scratches, the groove width is non uniform with signs of buckling, cracking along the edges of the scratch. A portion of cohesion failure can be observed in Fig. 14 (a) and (e) while in all others, adhesive layers seems to be completely delaminated from substrate surface. The defects at the edges of these scratches shows higher probability of substrate failure.

A dissimilar pattern was observed in A2/D2, as shown in Fig. 15, that there is dark lining inside the scratches in Fig. 15 (a), (b), (d) and (e). This area might have appeared due to point pressure caused by indenter during its motion and the variation can be seen increasing with the increasing load [Fig. 15 (f)]. Since (c) has minimum load, therefore, this pressure effected area was not dominating in this groove. Additionally, this indicates there is possibility of adhesion failure in higher loading conditions for such samples.

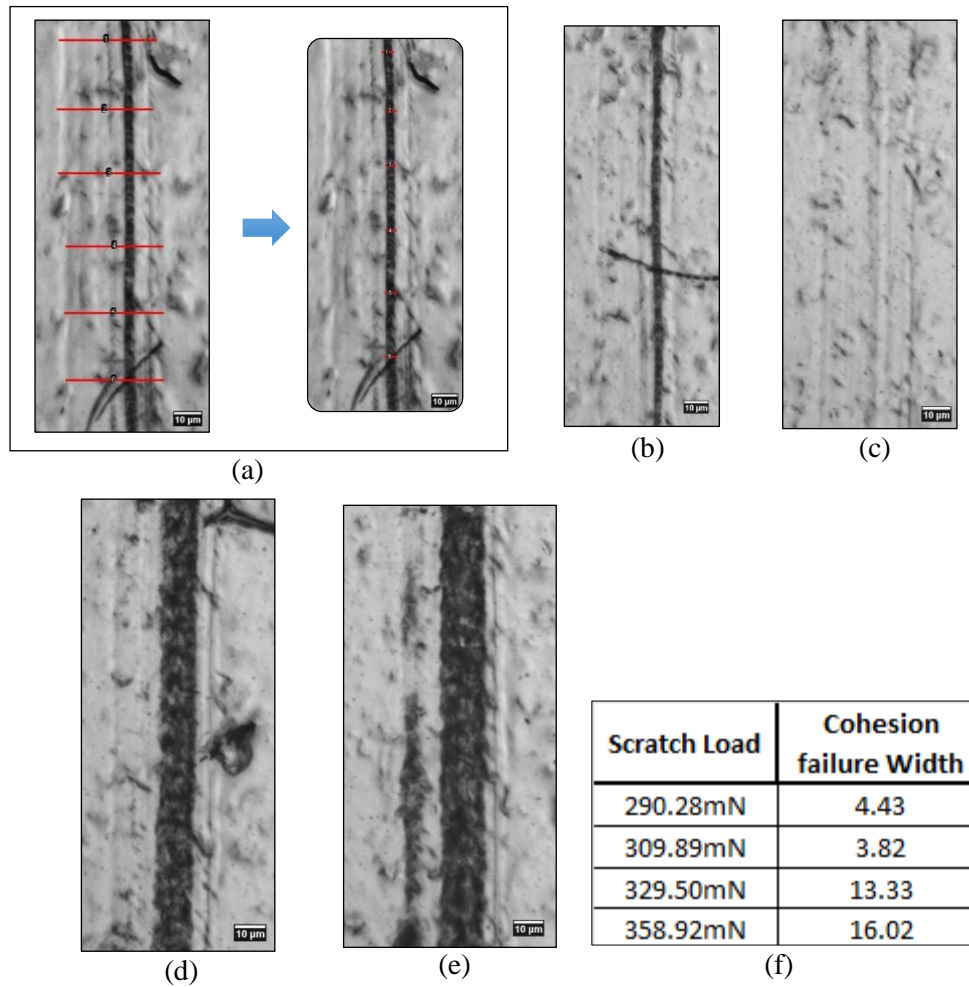
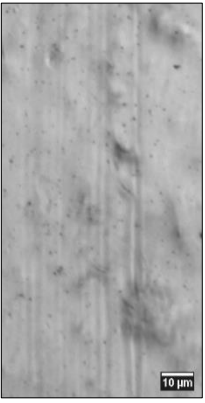
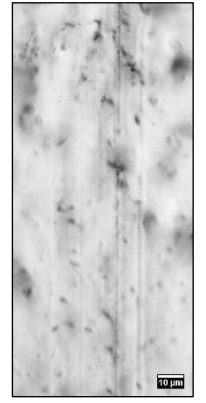
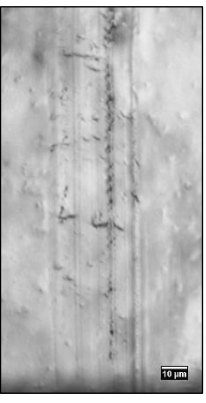

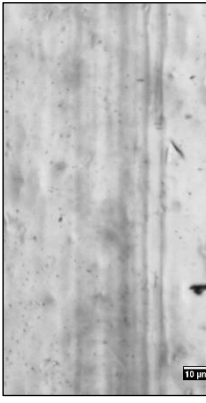
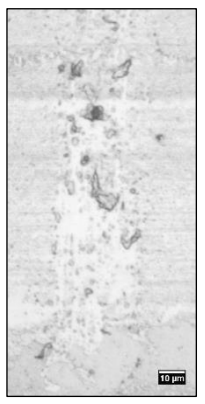
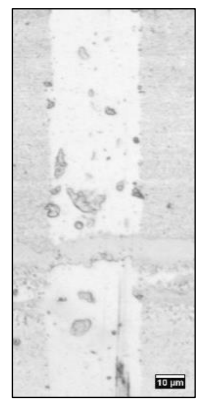

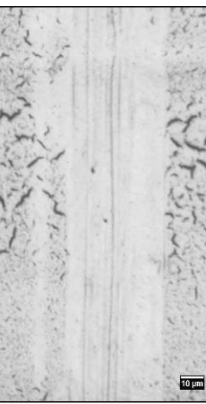
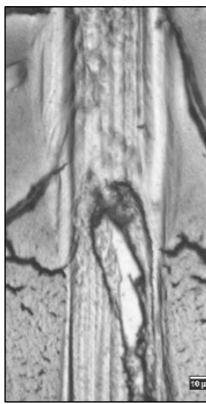
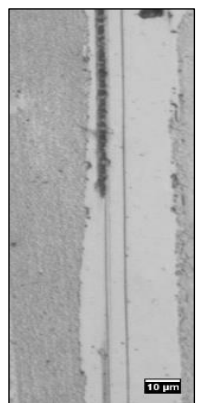
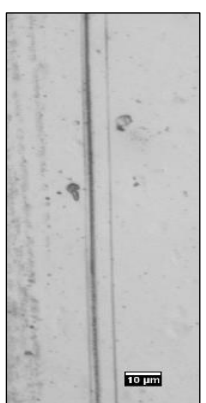


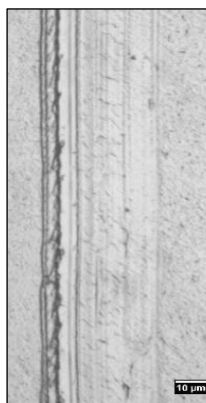

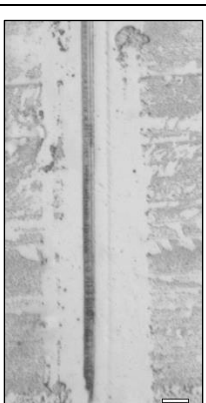

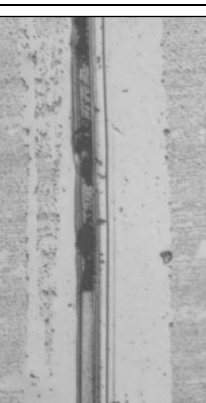
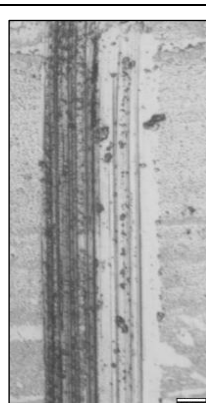


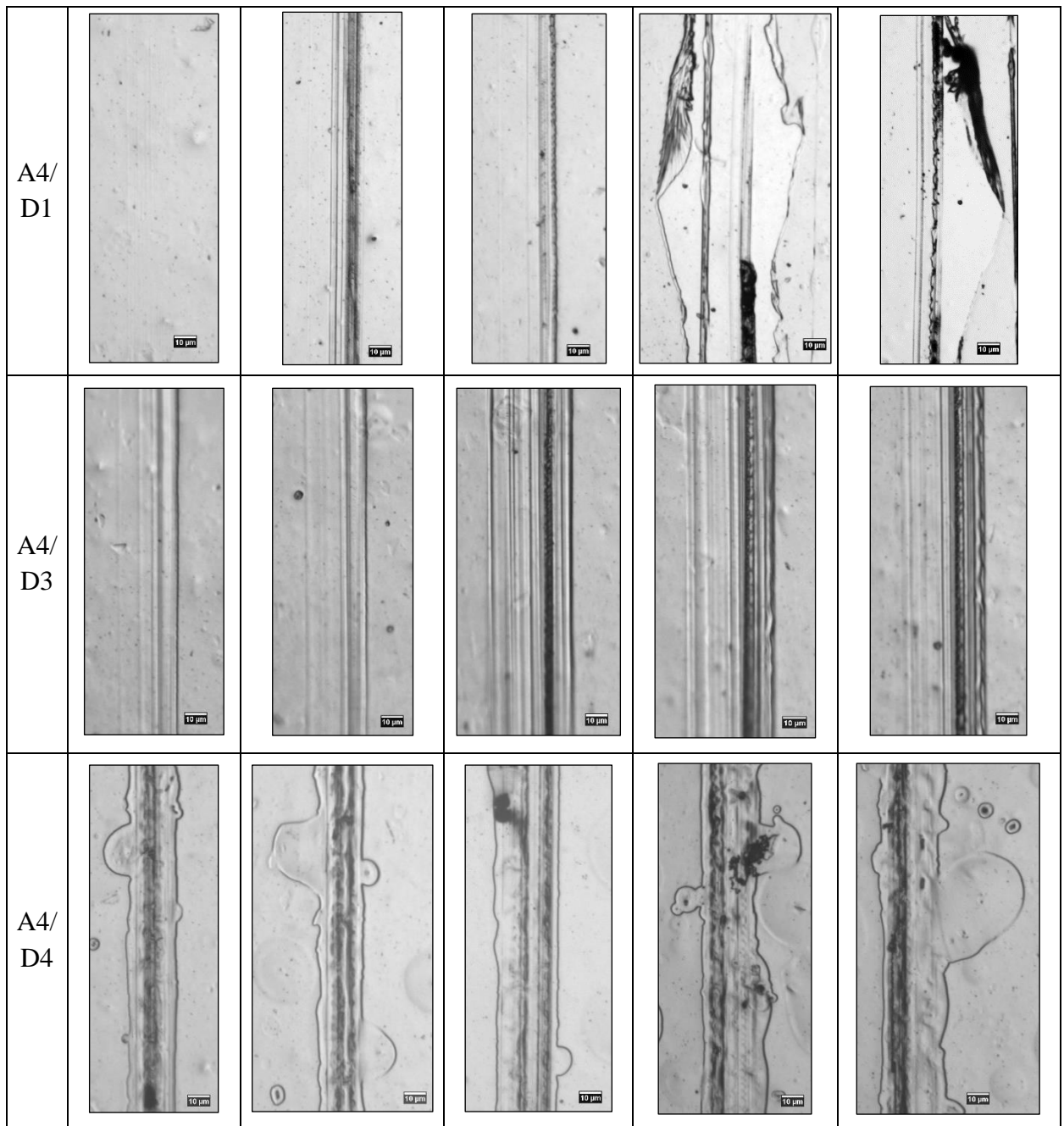
Fig. 15. Multilayer structures for sample adhesive A2 at rod diameter 14µm under scratch loads (a) – 309.89mN (b) – 290.28mN (c) – 260.86mN (d) – 329.5mN (e) – 358.92mN (f) – Cohesion failure width

Following all these observations so far, the rest of the samples can be explained using same concepts and measurement methodology. Table 7 collectively displays all scratch profiles of the remaining samples.

Table 7. Scratch profiles of samples with respect to scratch loads

Sample	260.86mN	290.28mN	309.89mN	329.5mN	358.92mN
A2/ D3					

A2/ D4	 <p>Micrograph showing surface texture of A2/D4, column 1. A 10 µm scale bar is present in the bottom right corner.</p>	 <p>Micrograph showing surface texture of A2/D4, column 2. A 10 µm scale bar is present in the bottom right corner.</p>	 <p>Micrograph showing surface texture of A2/D4, column 3. A 10 µm scale bar is present in the bottom right corner.</p>	 <p>Micrograph showing surface texture of A2/D4, column 4. A 10 µm scale bar is present in the bottom right corner.</p>	 <p>Micrograph showing surface texture of A2/D4, column 5. A 10 µm scale bar is present in the bottom right corner.</p>
A3/ D3	 <p>Micrograph showing surface texture of A3/D3, column 1. A 10 µm scale bar is present in the bottom right corner.</p>	 <p>Micrograph showing surface texture of A3/D3, column 2. A 10 µm scale bar is present in the bottom right corner.</p>	 <p>Micrograph showing surface texture of A3/D3, column 3. A 10 µm scale bar is present in the bottom right corner.</p>	 <p>Micrograph showing surface texture of A3/D3, column 4. A 10 µm scale bar is present in the bottom right corner.</p>	 <p>Micrograph showing surface texture of A3/D3, column 5. A 10 µm scale bar is present in the bottom right corner.</p>
A3/ D4	 <p>Micrograph showing surface texture of A3/D4, column 1. A 10 µm scale bar is present in the bottom right corner.</p>	 <p>Micrograph showing surface texture of A3/D4, column 2. A 10 µm scale bar is present in the bottom right corner.</p>	 <p>Micrograph showing surface texture of A3/D4, column 3. A 10 µm scale bar is present in the bottom right corner.</p>	 <p>Micrograph showing surface texture of A3/D4, column 4. A 10 µm scale bar is present in the bottom right corner.</p>	 <p>Micrograph showing surface texture of A3/D4, column 5. A 10 µm scale bar is present in the bottom right corner.</p>
A3/ D5	 <p>Micrograph showing surface texture of A3/D5, column 1. A 10 µm scale bar is present in the bottom right corner.</p>	 <p>Micrograph showing surface texture of A3/D5, column 2. A 10 µm scale bar is present in the bottom right corner.</p>	 <p>Micrograph showing surface texture of A3/D5, column 3. A 10 µm scale bar is present in the bottom right corner.</p>	 <p>Micrograph showing surface texture of A3/D5, column 4. A 10 µm scale bar is present in the bottom right corner.</p>	 <p>Micrograph showing surface texture of A3/D5, column 5. A 10 µm scale bar is present in the bottom right corner.</p>



The sample A2/D3 shows exactly same pattern as in A2/D2 with a little less dense impression. Same groove width measurement technique has been used and results are depicted in the next subsection. Furthermore, in A2/D4, the indenter did not penetrate much deeper into the layer and the scratch pattern looks almost similar in all the loading conditions. There are traces of cohesive failure but no adhesion failure, that means, this sample has good adhesive strength.

In case of A3/D3, all the scratch patterns are entirely different from each other. As seen from the table, 309.89mN load has completely peeled off the adhesive layer at some places while distorted at other places, that means, it possess gross spallation effect, meaning, large detached regions. Generally, it happens due to lack of adhesive strength. Whilst, 290.28mN and 260.86mN have buckling (irregular missing patches) failure along with gross spallation. 329.5mN load has comparatively large groove width, which means the loading is sufficient to damage the layer. Moreover, in 358.92mN, regions of detached coating can be seen accumulated along the sides of

stylus motion path. The reason behind this is plastic deformation of the substrate material accompanied by elastic recovery of adhesive layer after stylus passed through it. The next combination is A3/D4 which has a varied groove width among the scratches. To start with, 309.89mN shows regular groove width and signs of elastic recovery of the adhesive layer along the traces of stylus. There is no sign of adhesive failure but significantly damaged cohesive layers. On the other hand, 290.28mN and 260.86mN have smallest groove width out of all and the detached layer deposition can be seen along one side of the groove, which is termed as chipping (or recovery). 329.5mN shows removal of top most cohesive layer and no signs of adhesion failure. 358.92mN has depositions along the left side of the movement of stylus.

In A3/D5, the adhesive layer is completely wiped by the indenter in all cases. Moreover 309.89mN, 290.28mN, 329.5mN and 358.92mN show signs of substrate failure and the width of penetration into the substrate surface increases from 32.8 μ m to 48.29 μ m with increasing loads, however the groove width remains almost intact.

The next case, A4/D1 is an absolute representation of effect of increasing stylus load on the adhesive layer. 309.89mN and 290.28mN have similar as observed in A2/D4 329.5mN. In both scratches cohesive layer has been destroyed and elastic recovery can be seen along the right side of scratch. As the weight reduces to IW-5, the scratch impression becomes hardly noticeable as seen in 260.86mN. However, in higher loading conditions: 329.5mN and 358.92mN, the layer has been completely tore apart accompanied by acute signs of substrate failure.

A4/D3 projects cohesion failure in all five scratches. 290.28mN and 260.86mN have scratch impression only on the top surface of adhesive layer while 309.89mN, 329.5mN and 358.92mN have deeper and wider marks of penetration such that there are higher chances of substrate failure.

A4/D4 shows signs of adhesion failure because even the smallest load was able to penetrate deeper into the layer and may lead to substrate failure. There are bubble like structures along the edge of the groove which possibly indicates elastic recovery of adhesive particles which gets stick to the edges after the stylus passes. Fig. 16 shows dimensioning of scratches, taking into consideration total width of the bubbles formed.

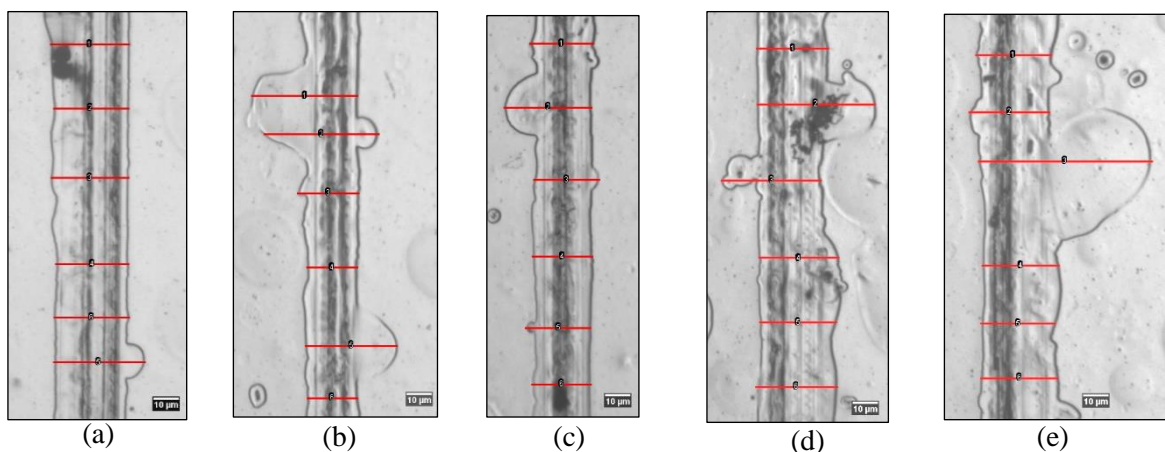


Fig. 16. Elastic deformation dimensions for scratch load (a) – 309.89mN (b) – 290.28mN (c) – 260.86mN (d) – 329.5mN (e) – 358.92mN

These scratches not only have extended elastic recovery but also cohesive penetration as observed in earlier cases. Thus further analysis is needed to clarify the performance of this combination which is discussed later in this chapter.

The graph showing plots of observed scratch widths for all five scratch loads at chosen rod wire diameter for adhesive A1 is depicted in Fig. 17. This variation shows scratch hardness tolerance of adhesive layer with respect to the applied loads, thereby, defining mechanical characteristic of the samples.

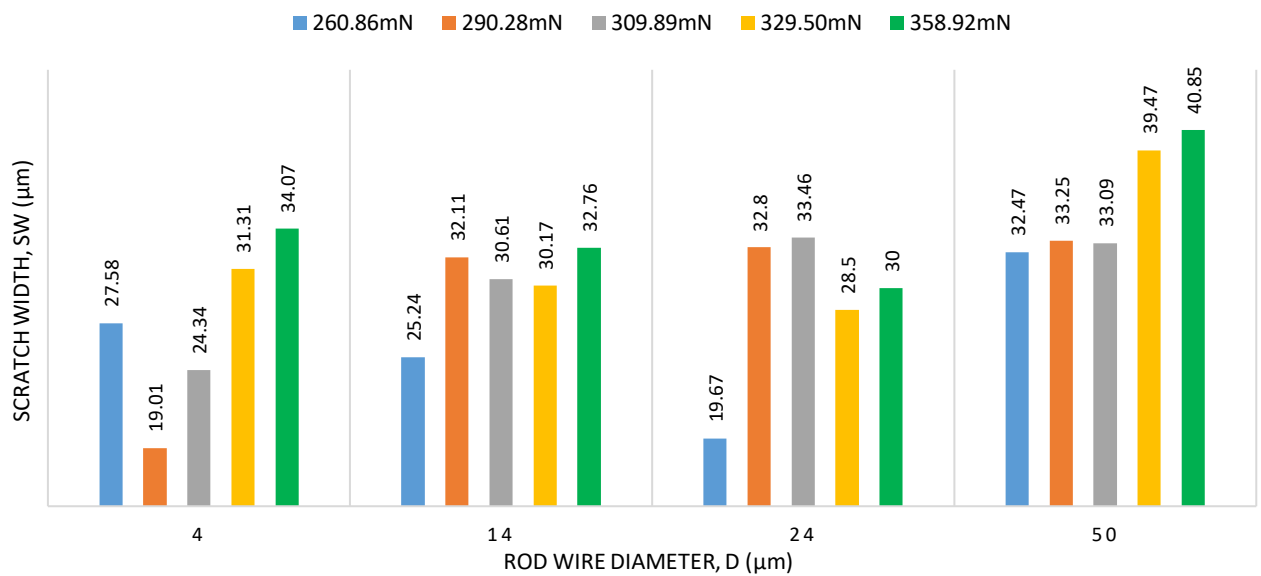


Fig. 17. Effect of scratch load on groove widths for multilayered structure with adhesive A1

Fig. 17 shows variation of scratch response with the load at different rod diameters. It is observed that there is an untraceable width pattern but in general higher load, $S = 358.92\text{mN}$ at diameter, $T = 50\mu\text{m}$ has the widest widths. The other loads have variable impact on scratch width and thus makes it practically independent on the loads.

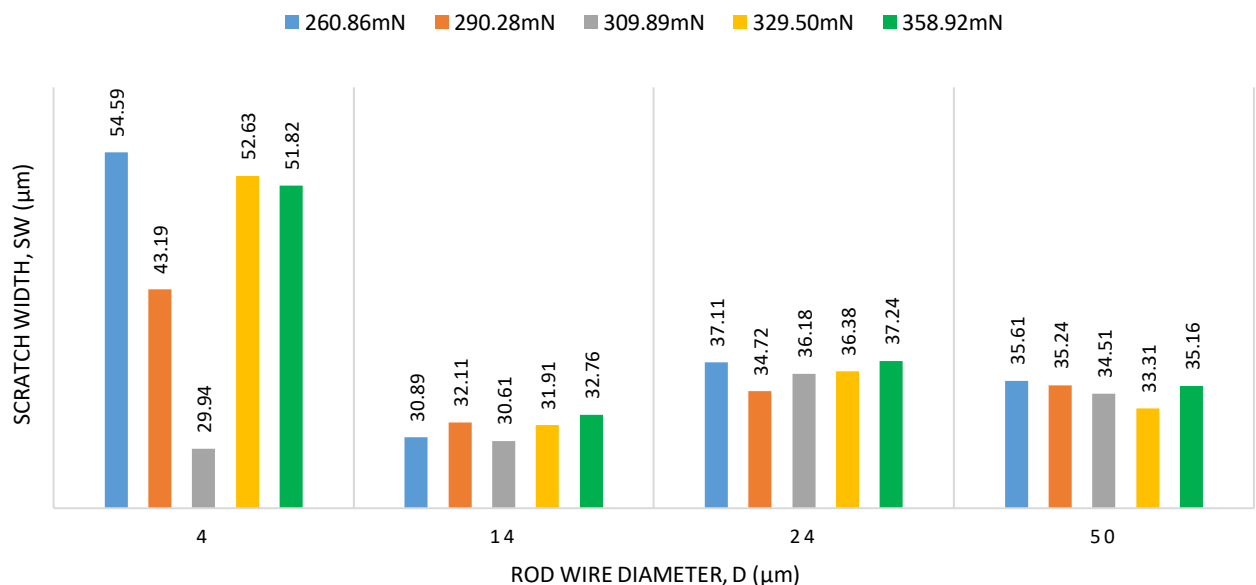


Fig. 18. Effect of scratch load on groove widths for multilayered structure with adhesive A2

Fig. 18 shows width variation for adhesive A2. Here, widths at higher loads, $S = 329.5$ and 358.92mN are not the widest unlike in adhesive A1, instead at load, $S = 309.89\text{mN}$ at diameter, $T = 4\mu\text{m}$ has more wider widths, indicating sensitivity response to lower thickness regime.

The scratch width dependence on scratch load for adhesive A3 has been shown in Fig. 19. Here, scratch widths first decrease from diameter, $T = 24\mu\text{m}$ to $50\mu\text{m}$ and then again increase till $T = 80\mu\text{m}$. In this case, width at load, $S = 329.5\text{mN}$ dominates than $S = 358.92\text{mN}$ at diameter $T = 24\mu\text{m}$ while at diameter $T = 50\mu\text{m}$ load $S = 309.89\text{mN}$ shows highest width.

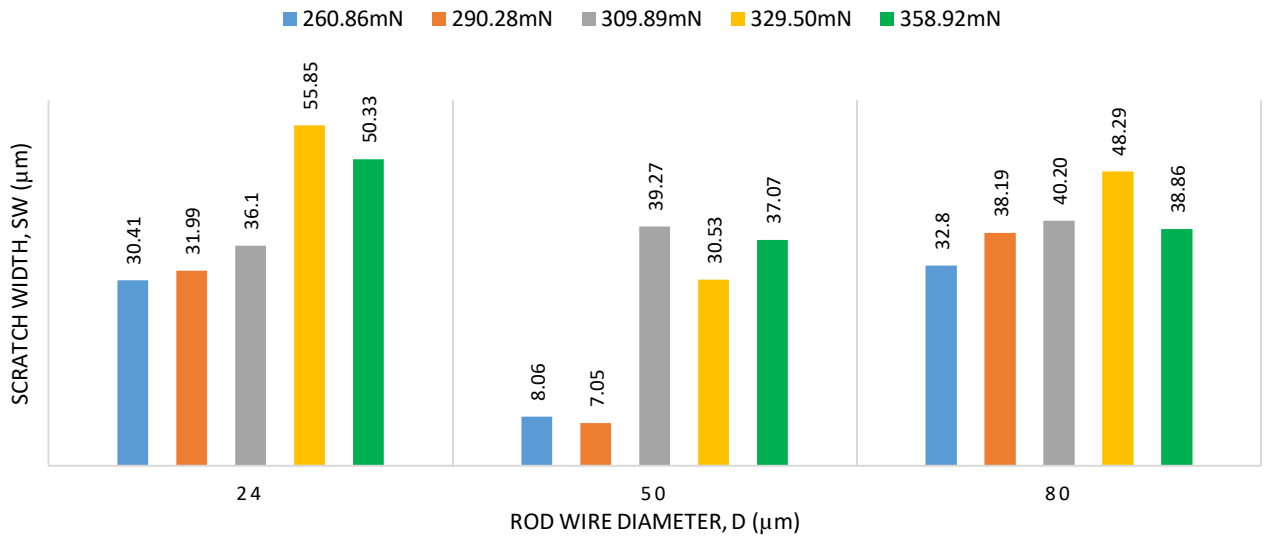


Fig. 19. Effect of scratch load on groove widths for multilayered structure with adhesive A3

In case of adhesive A4, as shown in Fig. 20, scratch widths first increases from $T = 4$ till $24\mu\text{m}$ and then falls down at $T = 50\mu\text{m}$. For individual thicknesses, it is observed that at smaller loads, $S = 260.86$ and 290.28 mN the widths are lesser in comparison to widths at higher loads. At $T = 4\mu\text{m}$, scratch loads are less likely to make impact on scratch widths in comparison to other diameters which explains that there is less internal resistance from adhesive layer and most of the load is transferred to the substrate.

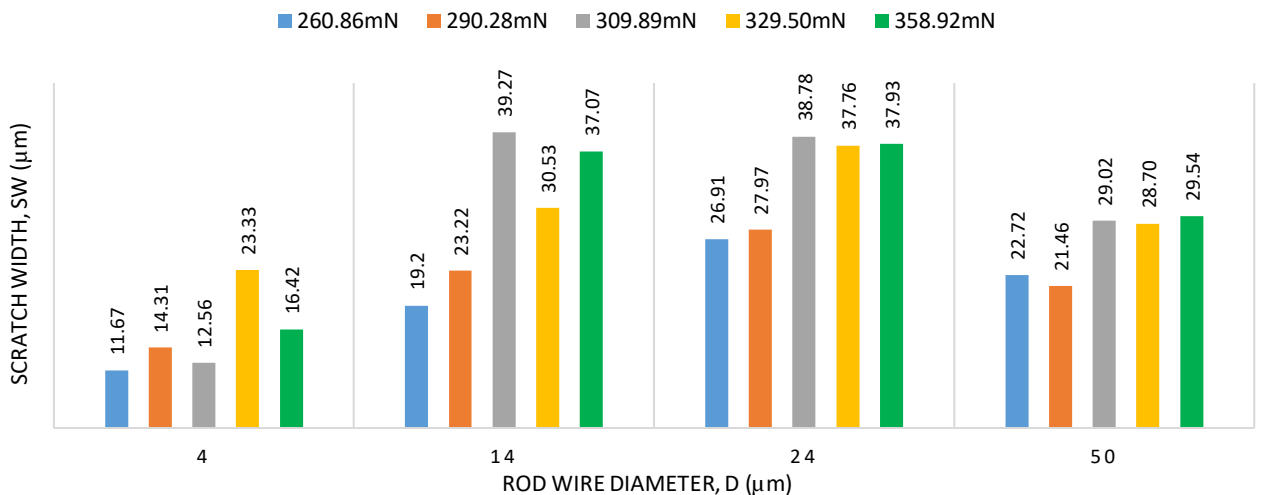


Fig. 20. Effect of scratch load on groove widths for multilayered structure with adhesive A4

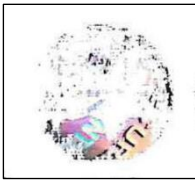


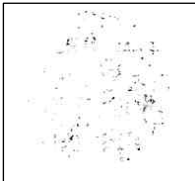











From scratch analysis, it was concluded that there is no significant dependence of scratch widths on scratch loads for any thickness. There are many more factors responsible for this variation apart from adhesive layer thickness.




3.4. Evaluation of quality of hot stamped periodical structures

In order to evaluate influence of adhesive layer, hot stamping is performed at different temperatures on paper (weighing 80g/m²) as substrate. These stamped structures were then evaluated on the basis of visual appearance. For instance, stamps size must be equivalent to diameter of dye (d = 19mm), should be homogenous and no distortion or defect in visibility of periodic structure. To make evaluation easier, the samples were divided into two groups, one with temperature range 90°C to 113°C and the other with 73°C to 106°C.

Table 8 and Table 9 indicate scanned stamped structures at corresponding temperatures. It can be seen that some structures are completely distorted as in case of A2/D1, some are partially stamped (A1/D1), some have imperfections at the edges (A4/D2) and only a few have complete profile with minimum or no visual defects as in A2/D4. From these results, the structures with defects were disregarded for scratch testing because of the visual deformity.

Table 8. Typical views of hot stamped structures at temperatures 90°C, 106°C and 113°C













Sample	Temperature (°C)		
	90	106	113
Adhesive A1 at rod diameter D1			
Adhesive A2 at rod diameter D1			
Adhesive A4 at rod diameter D1			
Adhesive A4 at rod diameter D2			
Adhesive A4 at rod diameter D3			
















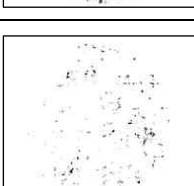


Adhesive A3 at rod diameter D4			
--------------------------------	---	--	---

The first three rows in Table 8 represent sample combination of adhesives A1, A2 and A4 with rod diameter D1 each. Clearly, the structures are highly distorted even at the highest stamping temperature, denoting poor quality. It might have occurred due to least retention of adhesive because of lower rod diameter. However, in case of adhesive A4 with rod diameter D2 and D3, distortion was observed only at the edges of the stamp which means the stamping time is not sufficient for proper adhesion of structure. And for adhesive A3 with D4, it can be said that this adhesive is sensitive to high temperatures, therefore, amount of distortion can be seen increasing with temperature. One possible reason could be low viscosity of this adhesive because of which the adhesive might be over heated, causing high intermolecular motion and could not adhere to the structure properly.

Some sample showed good visual structure after hot stamping even at lower temperature, 73°C as shown in Table 9. The evaluation was based on inspection under magnifying glass which resulted in a few samples recorded with good quality structures and those were selected as samples for comparison between high quality and low quality structures as shown in Table 10.

Table 9. Typical views of hot stamped structures at temperatures 73°C, 90°C and 106°C



Sample	Temperature (°C)		
	73	90	106
Adhesive A1 at rod diameter D2			
Adhesive A1 at rod diameter D3			
Adhesive A1 at rod diameter D4			
Adhesive A2 at rod diameter D2			





Adhesive A2 at rod diameter D3			
Adhesive A2 at rod diameter D4			
Adhesive A3 at rod diameter D3			
Adhesive A3 at rod diameter D5			
Adhesive A4 at rod diameter D2			
Adhesive A4 at rod diameter D4			

The common defects observed out of inspection of all samples were wavy edges, partly delaminated structures and no visual at all. Some of these defects were visible by naked eyes while others required magnification such that even smaller gaps could be seen on the overall surface area.

Table 10 shows comparison between good quality and bad quality structures to be selected for further analysis.

Table 10. Comparison between good and bad quality hot stamped structures

Sample	High quality	Sample	Low quality	Difference
Adhesive A2 at rod diameter D2 Temp: 106		Adhesive A3 at rod diameter D5 Temp: 90°C		Irregularity at the edges

Adhesive A2 at rod diameter D3 Temp: 106°C		Adhesive A4 at rod diameter D2 Temp: 90°C		Distortion at edges as well as surface
Adhesive A2 at rod diameter D4 Temp: 106°C		Adhesive A2 at rod diameter D4 Temp: 73°C		Irregularity on the surface

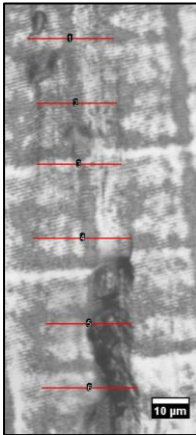
Based on the comparison from good quality structures, some high quality structures were selected for scratch analysis which are listed in Table 11.

Table 11. Samples selected for scratch testing

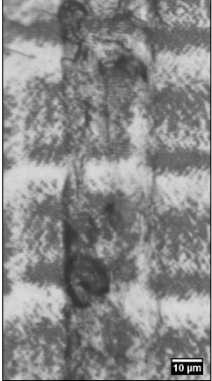
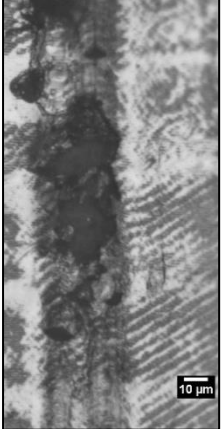

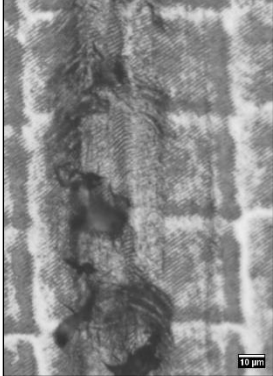
Sample	Temperatures (°C)
Adhesive A1 at rod diameter 14µm	106°
Adhesive A1 at rod diameter 24µm	73°, 90°, 106°
Adhesive A1 at rod diameter 50µm	73°, 90°
Adhesive A2 at rod diameter 14µm	106°
Adhesive A2 at rod diameter 24µm	106°
Adhesive A2 at rod diameter 50µm	90°, 106°
Adhesive A4 at rod diameter 50µm	106°

On the selected samples, scratch analysis was conducted so as to obtain a comparative evaluation of quality of hot stamped periodical structures. In this analysis, the obtained scratch profiles were entirely different from those observed in previous scratch analysis but the method of measurement of scratch width was same with some additional information on the profiles. Table 12 shows results of scratch test for adhesive A1 at rod diameter 14µm at temperature 106°C.

Table 12. Scratch views for adhesive A1 at rod diameter 14µm at 106°C

Scratch Load	106° C	Groove Width (µm)
260.86mN		33.78

Continued for Table 12

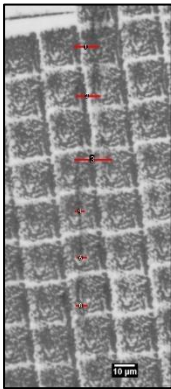

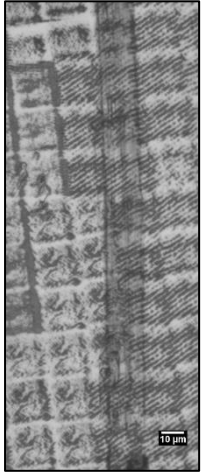
290.28mN		29.08
309.89mN		34.83
329.5mN		35.73
358.92mN		58.84

From Table 12, it was observed that scratch width increases from 29.08 to 58.84 μm with increasing scratch load. There is deformation recorded at the topmost layer of the structure in each case which might be due to surface roughness of substrate leading to abrasion wear at specific places only. Moreover, the wear is confined within the scratch boundary and there is no formation of wedges or cracks. In case of higher loads, for 329.5mN and 358.92mN, signs of elastic recovery of structure

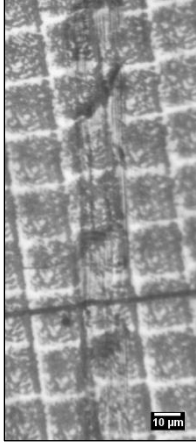
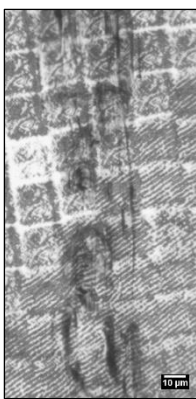
could be seen but the overall profile shows plastic deformation which indicates wear tolerance of this structure.

Similarly, scratch profiles were recorded for adhesive A2 at rod diameter 14 μ m at 106 $^{\circ}$ C and results are displayed in Table 13. The width of scratches varies in dissimilar manner as observed in previous sample. Here, width under load 290.28mN exceeds widths of 309.89mN and 329.5mN which is unusual. In this sample, for smaller loads like 290.28mN and 260.86mN, minor deformation is observed at the topmost layer.

Table 13. Scratch views for adhesive A2 at rod diameter 14 μ m at 106 $^{\circ}$ C

Scratch load	106 $^{\circ}$ C	Groove Width (μ m)
260.86mN	 A scanning electron micrograph showing a grid-like surface structure. A vertical scratch is visible, with several red arrows pointing to its edges. A 10 μ m scale bar is located at the bottom right.	8.76
290.28mN	 A scanning electron micrograph showing a grid-like surface structure. A vertical scratch is visible, appearing wider than the one at 260.86mN. A 10 μ m scale bar is located at the bottom right.	19.60
309.89mN	 A scanning electron micrograph showing a grid-like surface structure. A vertical scratch is visible, appearing wider than the one at 290.28mN. A 10 μ m scale bar is located at the bottom right.	16.16

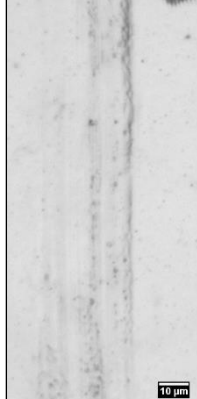

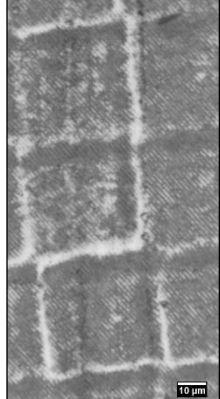
Continued for Table 13



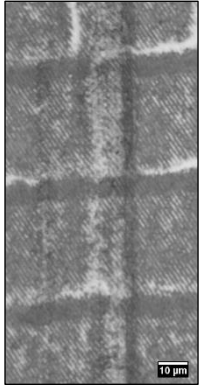
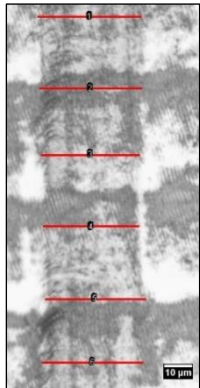
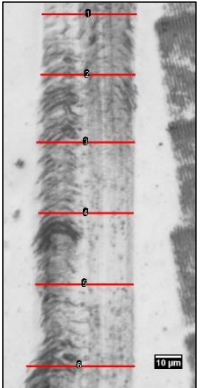
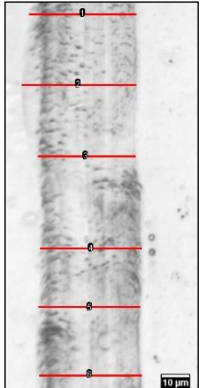
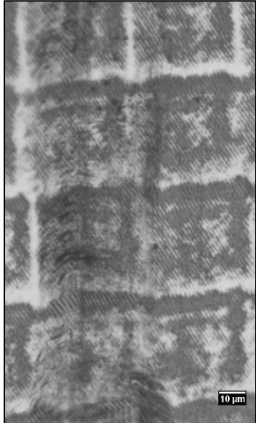

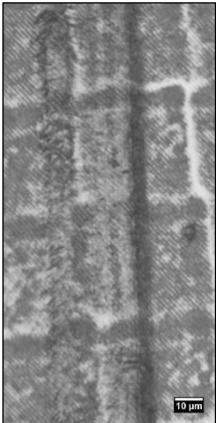
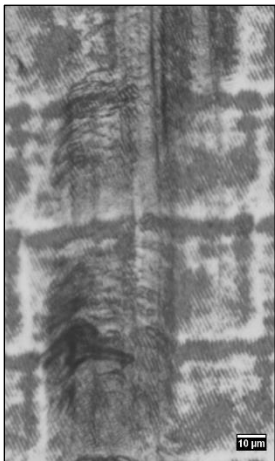
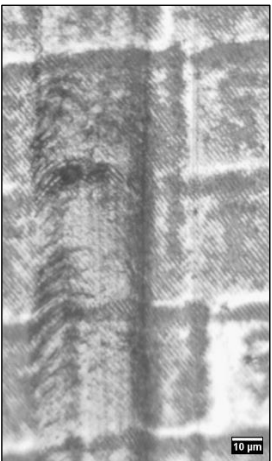
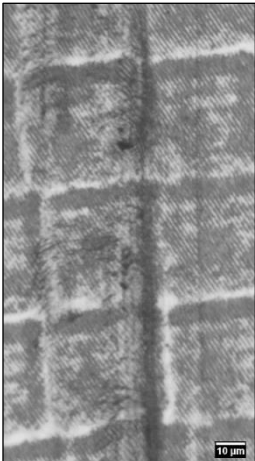
329.5mN		18.89
358.92mN		32.87

The widths obtained (Table 13) are significantly less than previous sample ranging from 8.76 μ m to 32.87 μ m from 260.86mN to 358.93mN respectively. Then in 309.89mN deformation intensifies with removal of topmost layer, leaving elastic recovery marks along the motion path of indenter. And for higher loads, 329.5mN and 358.92mN, bulging is observed in the scratched area but less severe as compared to previous case. At 358.92mN, the deformation seems more dense than other loadings which explains linear dependence of scratch on this structure to applied loads.

Table 14 shows scratch patterns for adhesive A1 at rod diameter 24 μ m at temperatures 60°C, 73°C and 90°C. Here, almost similar patterns were observed at different scratch loads in all three cases.

Table 14. Scratch views for adhesive A1 at rod diameter 24 μ m at 60°C, 73°C and 90°C

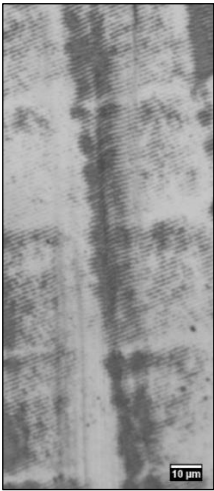
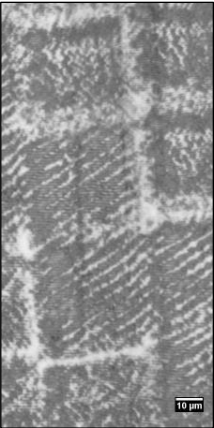
Scratch load	60°C	73°C	90°C
260.86mN	 <p style="text-align: center;">GW = 29.93μm</p>	 <p style="text-align: center;">GW = 32μm</p>	 <p style="text-align: center;">GW = 25.71μm</p>

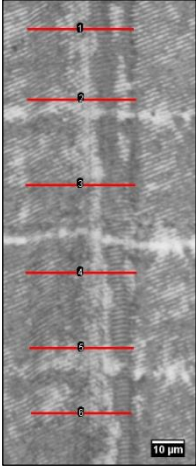
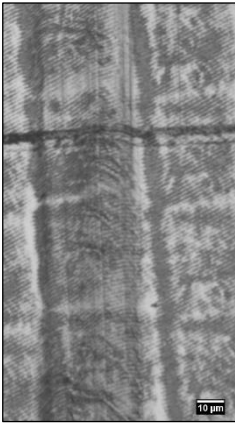
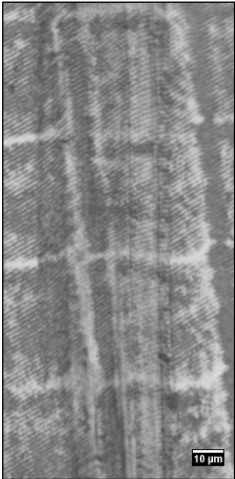
<p>290.28mN</p>	 <p>GW = 17.28μm</p>	 <p>GW = 33.82μm</p>	 <p>GW = 32.08μm</p>
<p>309.89mN</p>	 <p>GW = 34.87μm</p>	 <p>GW = 36.62μm</p>	 <p>GW = 36.90μm</p>
<p>329.5mN</p>	 <p>GW = 60.18μm</p>	 <p>GW = 53.45μm</p>	 <p>GW = 36.74μm</p>
<p>358.92mN</p>	 <p>GW = 58.27μm</p>	 <p>GW = 53.65μm</p>	 <p>GW = 54.30μm</p>

At 260.86mN and 290.28mN minimal cohesive deformation was observed at the topmost layer but wedges started to appear along the scratch edges as the load increases to 309.89mN in all three cases. At temperature 73°C, there is buckling phenomenon observed along the left edge of scratch at load 309.89mN. Similarly at 329.5mN and 358.92mN, buckling and wedging was observed in both 63°C and 73°C while minor abrasion wear was observed along the indenter motion path in case of 90°C. Among three temperatures, 90C showed better adhesive quality than the other two in terms of groove width as well as effect of scratch load. The groove widths for 60°C were larger than at 73°C and 90°C with maximum groove width of 60.18µm while that at 73°C with 53.65µm and 90°C with 54.30µm. It shows that at lower temperatures internal stresses are less dominant therefore, the periodical structure shows signs of cracking.

The next sample, adhesive A2 at rod diameter 24µm at 106°C is represented in Table 15. The results observed in this case were most promising in terms of scratch tolerance by the periodical structure. The first three scratches, at 309.89mN 290.28mN and 260.86mN do not indicate significant surface deformation but the marks of indenter motion path were visible. At loads 329.5mN and 358.92mN, wider groove width was observed with wedge formation along the line of motion of indenter and signs of structure failure at higher loads.

Table 15. Scratch views for adhesive A2 at rod diameter 24µm at 106°C

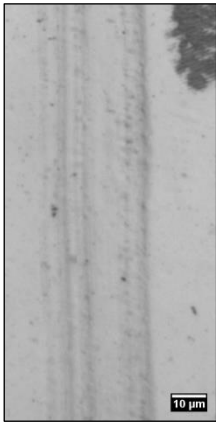
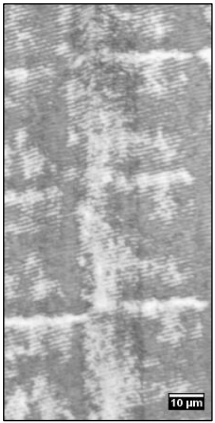
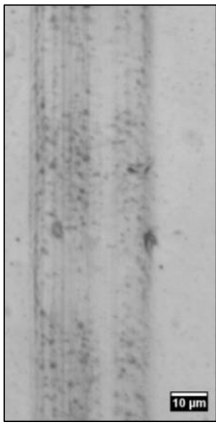
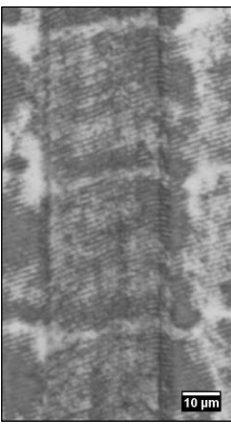
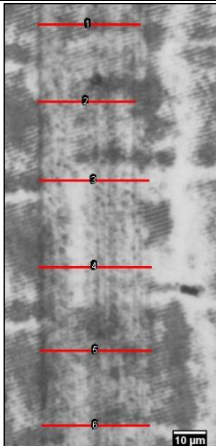
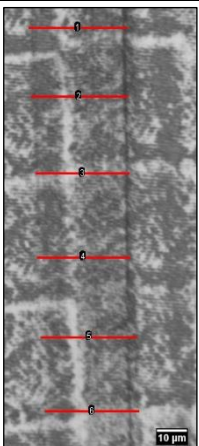

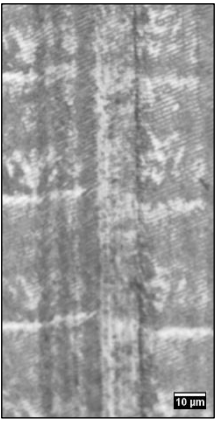
Scratch load	106°C	Groove Width (µm)
260.86mN		28.05
290.28mN		30.7


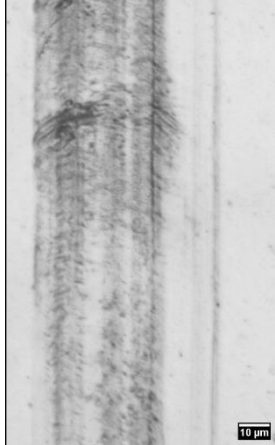
309.89mN		32.68
329.5mN		41.4
358.92mN		41.16

Overall, this sample displayed good abrasive resistance and better adhesion as compared to other samples. This might be due to superior viscosity and high temperature that eliminated all internal stresses that must have been formed during coating and drying process.

Next sample, shown in Table 16, consists of adhesive A1 at rod diameter 50µm at two different temperatures 73°C and 90°C. The first one shows similar pattern as in previous sample, with clear scratch marks in all five cases. The groove width for 290.28mN load exceeds that of 309.89mN which may be because of higher resistance of printed structure in the later case while in former one no such hinderance is there. In case of 329.5mN and 358.92mN, deformation could be seen along the scratch edges accompanied with wedge formation.

Table 16. Scratch views for adhesive A1 at rod diameter 50 μ m at 73 $^{\circ}$ C and 90 $^{\circ}$ C

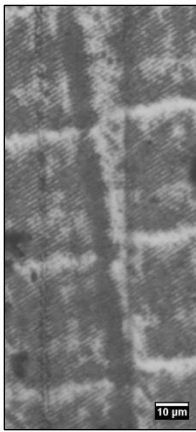
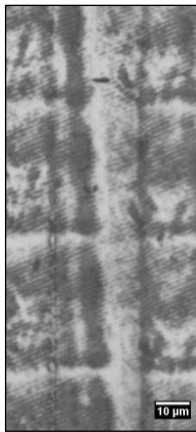
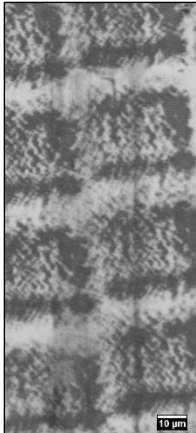

Scratch load	73 $^{\circ}$ C	Groove Width (μ m)	90 $^{\circ}$ C	Groove Width (μ m)
260.86mN		31.06		19.46
290.28mN		33.41		31.59
309.89mN		32.28		30.86
329.5mN		36.78		35.24

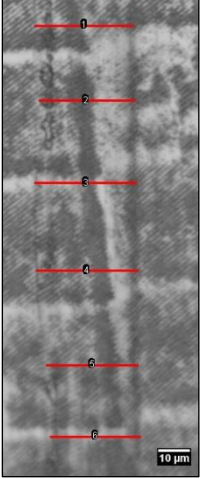
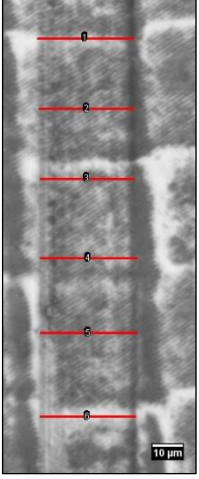
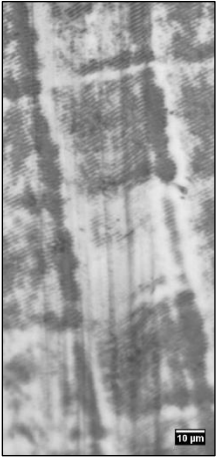
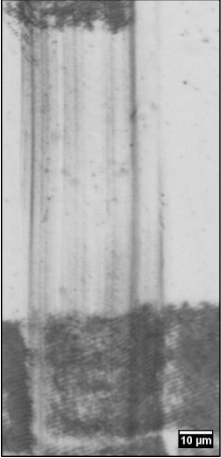
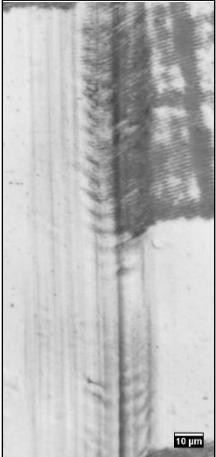
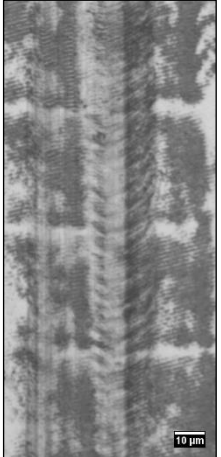
358.92mN		42.70		59.49
----------	---	-------	--	-------

In case of 90°C, groove widths are comparatively lesser in 309.89mN, 290.28mN, 260.86mN and 329.5mN but significantly large in 358.92mN, because of low surface hinderance. All scratches show clear cut motion path of indenter with no merging deformation except in 358.92mN load.

Table 17 displays scratch patterns for adhesive A2 at rod diameter 50µm at 90°C and 100°C. For 90°C case, nominal deformation was observed in 260.86mN, 290.28mN and 309.89mN while at higher loads 329.5mN and 358.92mN, buckling could be seen along the motion path of indenter. This might be due to high surface roughness as this adhesive has paste like structure unlike other adhesives.

Table 17. Scratch views for adhesive A2 at rod diameter 50µm at 90°C and 100°C

Scratch load	90°C	Groove Width (µm)	100°C	Groove Width (µm)
260.86mN		27.25		26.36
290.28mN		30.17		28.99

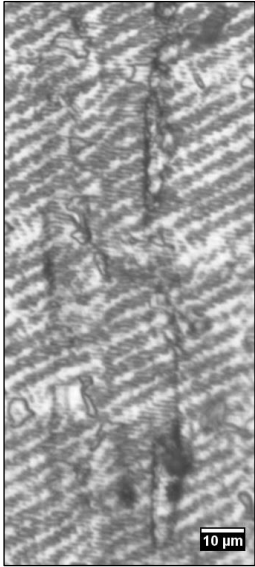

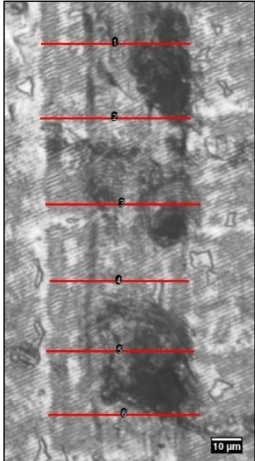
309.89mN		29.48		30.49
329.5mN		38.85		41.81
358.92mN		44.65		42.78

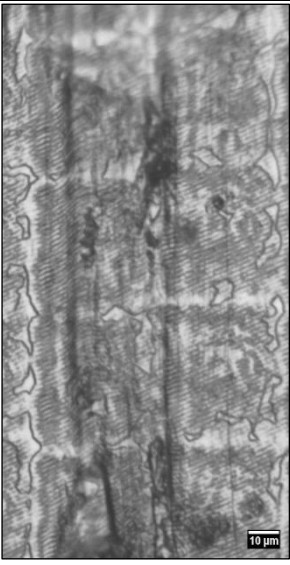
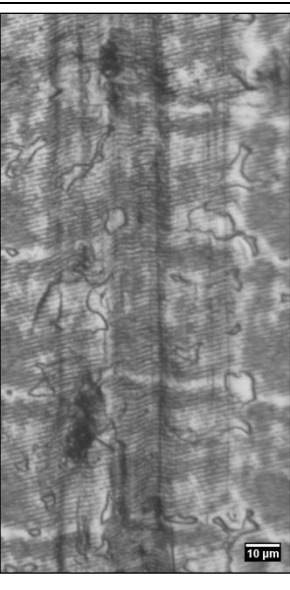
Similarly for 100°C, first four loads have top layer deformation but the last one has same effect as in 90°C. The groove width varies from 27.25 μm to 44.65 μm for 90°C while that in 100°C from 26.26 μm to 42.78 μm . Both samples have distinctive properties and it is not feasible to establish a mathematical relationship between scratch load to groove width from the observation.

The next sample as shown in Table 18, consists of adhesive A4 at rod diameter 50 μm at temperature 106°C, showed surface deformation and cracking in all five scratches. In general, all scratch loads had significant effect of adhesion failure on the periodic structure and the groove widths are also large ranging from 29.56 μm to 58.11 μm . For load 309.89mN, large cracking marks were observed along

the edge of scratch while at 260.86mN and 290.28mN comparatively smaller cracks were seen along the edge of scratch.

Table 18. Scratch views for adhesive A4 at rod diameter 50 μ m at 106 $^{\circ}$ C

Scratch load	106 $^{\circ}$ C	Groove Width (μ m)
260.86mN	 <p>A scanning electron micrograph showing a scratch on a surface. The scratch is a dark, irregular line. The surrounding surface has a fine, grid-like texture. A scale bar in the bottom right corner indicates 10 μm.</p>	29.56
290.28mN	 <p>A scanning electron micrograph showing a scratch on a surface. The scratch is a dark, irregular line. The surrounding surface has a fine, grid-like texture. A scale bar in the bottom right corner indicates 10 μm.</p>	51.26
309.89mN	 <p>A scanning electron micrograph showing a scratch on a surface. The scratch is a dark, irregular line. The surrounding surface has a fine, grid-like texture. Six horizontal red lines are drawn across the scratch, labeled with the letter 'a' at their ends. A scale bar in the bottom right corner indicates 10 μm.</p>	49.27

<p>329.5mN</p>		<p>58.11</p>
<p>358.92mN</p>		<p>50.08</p>

The groove widths are almost comparable at 290.28mN, 309.89mN and 358.92mN loads, measuring 51.26μm, 49.27μm and 50.08μm respectively, however, the deformation pattern is entirely different. All scratch widths are significantly high measuring from 29.56μm to 58.11μm and there is no correlation of groove width with loads applied because groove width at 329.5mN exceeds groove width at 358.92mN.

4. Recommendations

This case study was conducted as an attempt to provide improvization in the method of hot stamping in dependence with adhesive layer thickness. There are some possibilities discovered during the study which can enhance the existing process, for example, adhesive layer thickness and hot stamping temperature. In order to achieve better output, some other parameters can also be implied which were untouched in this study, like hot stamping press load, time duration of stamp because these parameters can significantly affect the productivity at mass level. So, there are still wide open opportunities in this area to be worked on.

5. Conclusion

The quality of hot stamped periodic structures in dependence of adhesive layer nature and thickness have been investigated.

1. The influence of coating rod diameters of $D = 4, 14, 24, 50$ and $80 \mu\text{m}$ and adhesive nature on the adhesive layer thickness formed on the multilayer polymeric film have been investigated.
 - 1.1. It was found that for adhesives A1 and A2 exist linear dependence between adhesive layer thickness and rod wire diameter. Increase of rod wire diameter resulted on the increase of adhesive layer thickness.
 - 1.2. Adhesive A3 was comparatively less viscous than A1 and A2, therefore the coated layer thickness dependence on rod wire diameter was uneven. Besides, thickness values were significantly lower than those found for adhesives A1 and A2. At $D = 50 \mu\text{m}$, the thickness value was $6.53 \mu\text{m}$ which exceeded the value at $D = 80 \mu\text{m}$ with $1.37 \mu\text{m}$ which is even smaller than the value at $D = 14 \mu\text{m}$ with $2.72 \mu\text{m}$.
 - 1.3. Adhesive A4 was solvent based adhesive with smallest concentration and viscosity out of all four samples. The coated layer thickness dependence vs rod diameter was found tend to decrease till rod wire diameter $D = 24 \mu\text{m}$ and then suddenly rises at $D = 50 \mu\text{m}$.
2. The scratch resistance of adhesive layers was evaluated with respect to adhesive layer formation regimes using five scratch loads, $S = 260.86, 290.28, 309.89, 329.5$ and 358.92 mN at constant speed of indenter motion.
 - 2.1. For adhesive A1, the scratch grooves width was observed lied between $19.01 \mu\text{m}$ and $40.85 \mu\text{m}$. The higher widths were observed in the sample with $D = 50 \mu\text{m}$ as compared to other diameters and the maximum width was observed at load, $S = 358.92 \text{ mN}$ at diameter, $D = 50 \mu\text{m}$ while the smallest width at load, $S = 290.28 \text{ mN}$ at diameter, $D = 4 \mu\text{m}$.
 - 2.2. For adhesive A2, the scratch grooves width lied between $29.94 \mu\text{m}$ and $54.59 \mu\text{m}$ and the higher widths were observed for diameter, $D = 4 \mu\text{m}$. The maximum width was observed at load, $S = 260.86 \text{ mN}$ at diameter, $D = 4 \mu\text{m}$ while the minimum at load, $S = 309.89 \text{ mN}$ at same diameter.
 - 2.3. For adhesive A3, scratch grooves width lied between $7.36 \mu\text{m}$ and $55.85 \mu\text{m}$ and maximum width was observed at load, $S = 329.5 \text{ mN}$ at diameter, $D = 24 \mu\text{m}$ while minimum width at load, $S = 290.28 \text{ mN}$ at diameter, $D = 50 \mu\text{m}$.
 - 2.4. For adhesive A4, scratch grooves width ranged from $11.67 \mu\text{m}$ to $39.27 \mu\text{m}$ with lowest width observed at load, $S = 260.86 \text{ mN}$ at diameter, $D = 4 \mu\text{m}$ while the maximum at load, $S = 309.89 \text{ mN}$ at diameter, $D = 14 \mu\text{m}$.
 - 2.5. From comparison, scratch groove width of adhesive A1 had minimum variation in measured values followed by A2, then A4 and finally A3. Statistically, it shows better results than other adhesives but considering the physical deformation observed, adhesive A2 at diameter, $D = 50 \mu\text{m}$ shows more promising results.
3. Periodical structures hot stamping quality in dependence of adhesive layer nature, thickness and hot stamping temperature have been investigated. was conducted.
 - 3.1. It was found that hot stamping quality depends on adhesive layer nature, its thickness and hot stamping temperature. Based on visual inspection, best quality of stamped structures were found in case of adhesive layer A1 ($D = 14 \mu\text{m}, T = 106^\circ\text{C}$; $D = 24 \mu\text{m}, T = 73^\circ, 90^\circ$,

106°C; D = 50µm; T = 73°, 90°C) adhesive layer A2 (D = 14µm, T = 106°C; D = 24µm T = 106°C; D = 50µm; T = 90°, 106° C) and for adhesive A4 at rod diameter D = 50µm and hot stamping temperature T = 106° C. These structures were selected for final evaluation.

- 3.2. Scratch groove width measurement results indicated same untraceable patterns as in case of adhesive layer, however the profiles show cracking of adhesive layer with increasing loads.
- 3.3. At smaller loads, S = 260.86 and 290.28 mN, there is very small or no deformation observed while in case of higher loads, S = 309.89, 329.5 and 358.92 mN, adhesive failure was observed.

6. List of References

1. **James, M. Long and D. Newcomb.** Designing security holograms. *Proceedings of SPIE*. 2004 m., 12.
2. **EBNESAJJAD, SINA.** Introduction and Adhesion Theories. *Adhesives Technology Handbook (2nd edition)*. s.l. : Elsevier Inc., 2011.
3. *Laser ablation of multilayered hot stamping foil.* **Leech, P. W.** 9, Victoria : Elsevier B.V., 2009 m., T. 209.
4. *Insights into adhesion of abalone: A mechanical approach.* **Jing Lia, Yun Zhangb, Sai Liub, Jianlin Liub.** 2018 m., Mechanical Behavior of Biomedical materials, p. 331-336.
5. **SATAS, D.** *Coatings Technology Handbook*. New York : Marcel Dekker Inc., 1991.
6. *Controlling of resin impregnation and interfacial adhesion in carbon fiber/polycarbonate composites by a spray-coating of polymer on carbon fibers.* **Ting-Ting Yao, Yu-Ting Liua, Hong Zhua, Xiao-Fang Zhang, Gang-Ping Wu.** 2019 m., Elsevier, p. 63-77.
7. *Analysis of the adhesion of Pseudomonas putida NCIB 9816-4 to a silica gel as amodel soil using extended DLVO theory.* **Geelsu Hwanga, Chang-Ha Leea, Ik-Sung Ahna, Byung Jin Mhin.** 2010 m., Journal of Hazardous Materials, p. 983–988.
8. *Carboxylated multiwalled carbon nanotubes effect on dynamic.* **Farzad Zahedi, Iraj Amiri Amraee.** 2018 m., Elsevier, p. 187-196.
9. *Structure and Growth Mechanism of V/Ag Multilayers with.* **Hongxiu Zhang, Feng Ren, Mengqing Hong, Xiangheng Xiao, Guangxu Cai.** 10, 2014 m., Elsevier, p. 1012-1019.
10. *Bonding quality assessment of cross-layered Maritime pine elements.* **Pedro Santos, João R. Correia, Luís Godinho, A.M.P.G. Dias, André Dias.** 2, 2019 m., Elsevier, T. 21, p. 571-582.
11. *Laser ablation of multilayered hot stamping foil.* **Leech, PatrickW.** 2009 m., Elsevier, T. 209, p. 4281–4285.
12. *Acidic hydrophobic nanosilica particle-induced mechanical.* **Hossein Yazdani-Ahmadabadia, Saeed Rastegara, Zahra Ranjbarb.** 2016 m., Elsevier, T. 100, p. 173-177.
13. *SEM observations of a metal foil laminated with a polymer film.* **Nasir Mehmoodb, Eskil Andreassona, Sharon Kao-Walter.** 2014 m., Elsevier, T. 3, p. 1435 – 1440.
14. *Solid state diffusion bonding characteristics at the interfaces of Ti and Al layers.* **A.H. Assari, B. Eghbali.** Tabriz : Elsevier Ltd., 2019 m.
15. *Microstructure and mechanical properties of Al-based metal matrix composites reinforced with Al₈₄Gd₆Ni₇Co₃ glassy particles produced by accumulative roll bonding.* **Saba Khoramkhorshid, Morteza Alizadeh, Amir Hossein Taghvaei, Sergio Scudino.** Dresden : Elsevier Ltd., 2016 m.
16. *Simulation method for precision bonding structure with analyze the functional and p.* **Xiao CHENa, Zhijing ZHANG, Xin JINa, Muzheng XIAO, Huan GUOa□Zhaoli.** 2018 m., Elsevier, T. 76, p. 100-105.
17. **CAMMARATA, ROBERT C.** Surface effects on intrinsic thin-film stresses. [knygos aut.] **KL MITTAL.** *Adhesion Aspects of Thin Films*. Baltimore : Taylor & Francis Group, 2005, p. 3-12.
18. *Properties of water-borne coating incorporate with nanoclay.* **U M K Anwar, S Y Alia, K Tumirah, H Hamdan and M T Paridah.** Malaysia : IOP Publishing, 2018. The Wood and Biofiber International Conference.

19. *Influence of water adhesion of superhydrophobic surfaces on their anticorrosive behavior.* **Mengke Cuia, Yongqian Shenb, Haifeng Tiana, Yaoxia Yanga, Hua Fenga, Jian Li.** Lanzhou : Elsevier Ltd., 2017 m.
20. *The effect of sandblasting on surface properties for adhesion.* **Anna Rudawska, IzabelaDanczak, MiroslavMüller, PetrValasek.** Praha : Elsevier Ltd., 2016 m.
21. *A modified scratch test for the mechanical characterization of scratch resistance and adhesion of thin hard coatings on soft substrates.* **T. Sander, S. Tremmel, S. Wartzack.** Erlangen : Elsevier Ltd., 2011 m.
22. *New and improved tests for adhesion.* **Gent, A. N.** 2006 m., The Journal of Adhesion, p. 115-122.
23. **Satas, D.** Adhesion Testing. *Coatings technology handbook.* New York : Marcel Dekker Inc., 1991.
24. *Quantitative evaluation of scratch resistance of polymeric coatings based on a standardized progressive load scratch test.* **R.L. Browning, G.-T. Lim, A. Moyse, H.-J. Sue, H. Chen, J.D. Earls.** 2006 m., Surface & Coatings Technology, p. 2970–2976.
25. **KADLÍČEK, Ing. TOMÁŠ.** SCRATCH TEST. *MICROMECHANICS AND MICROSTRUCTURAL DESCRIPTION.* 2015 m.